Currents in the Tasman Sea in a changing climate

Future changes to oceanic volume and temperature transports around Australia and New Zealand using New Zealand's Earth System Model.

Sylvaine Isolde (Liv) Cornelissen Bogers

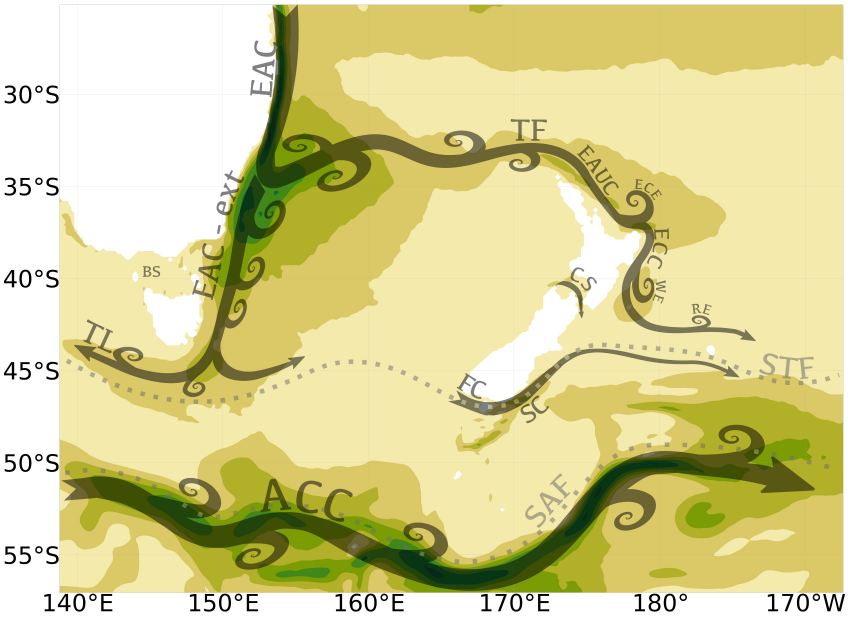

Master's Thesis
Climate Physics

October 2022

Supervisors

Dr. Erik Behrens
Prof Dr. Erik van Sebille
Dr. Siren Rühs

NIWA
Taihoro Nukurangi

Utrecht University

Contents

Figure 1: (Front page) The currents in the Tasman Sea, that are pictured here, are part of the Western Boundary Current system of the South Pacific ocean. The main currents are the East Australian Current (EAC) and EAC-extension, Tasman Front (TF), Tasman Leakage (TL), Antarctic Circumpolar Current (ACC), East Auckland Current (EAUC), East Cape Current (ECC), Southland Current (SC), Fjordland Current (FC), Cook Strait (CS), Bass Strait (BS). The persistent eddies are the East Cape eddie (ECE), Wairarapa Eddy (WE) and Rekohu Eddie (RE). The Subtropical Front (STF) and Subantarctic Front (SAF) are represented by the grey dotted line. The background field is the mean surface velocity of the historical simulation.

Abstract

Western boundary currents are an important element of the climate system since they control the oceanic meridional heat transport. Climate projections around Australia and New Zealand suggest an increase in volume transport of the Tasman Leakage but a decline for the Tasman Front, which carries water and heat towards New Zealand. Despite this decline, the region around the North Island of New Zealand has been identified as a region with extreme warming and this raises the question of what drives this warming. In this study we investigate climate projections of New Zealand's Earth System Model to quantify changes to transports of the oceanic currents and possible driver for the warming using low (SSP1-2.6), medium (SSP2-4.5) and high (SSP3-7.0) emission scenarios in combination with Lagrangian particle tracking analyses. The direction of change in volume transport agrees with previous studies. Our projections reveal an increase between 16% and 76% in volume transport and a 29% and 122% increase in temperature transport of the Tasman Leakage between the low and high emission scenarios. In the Tasman Front, volume transport for SSP2 and SSP3 scenarios decline between 10% and 33%. The temperature transport increases in SSP2 with 4% and decreases with 20% in SSP3. Therefore, a possible driver for the intensifying marine heat waves around the North Island of New Zealand could be the decrease in volume transport that allows for heat accumulation in the region. The Lagrangian analyses reveal that the temperature along the trajectory is projected to increase in the high emission scenario. At the end of the 20^{th} century only 1% of the volume weighted trajectories towards New Zealand are above 20°C, this increases to 5.5% by the end of the 21^{st} century for the high emission scenario. Despite a decline in the overall Lagrangian temperature transport, the volume weighted fraction of trajectories which encounter higher temperatures from the EAC to the north of NZ increases which possibly widens or opens up a pathway for tropical species towards NZ.

Acknowledgement

I would like to thank my supervisors Erik Behrens, Erik van Sebille and Siren Rühs for the help during my research and writing my thesis. Erik Behrens, I have learned a lot from our conversations and discussions in our meetings. I appreciate that you listened to my sometimes big and creative ideas and helped me to focus them based on your extensive knowledge, so they would be feasible within the time frame of my thesis. You have given me enough freedom so I could figure out needed tools and next steps in my research on my own, but also gave me the guidance I needed to make my thesis a successful research project. I'd like to thank Erik van Sebille for his supervision from the other side of the world. I learned a lot from your knowledge on the Lagrangian transports and OceanParcels that you shared in video calls and in the meeting we had when I was at the Utrecht University. Siren, thank you for all our meetings via Teams and the day working together in Utrecht. You patiently answered all my countless questions about the underlying theory and mechanisms of Lagrangian transport. I enjoyed our scientific discussions and our personal chats. I also want to thank Paul Groos for checking the grammar and spelling of my thesis. And for being a good friend who I could always share my ups and downs with.

Furthermore, I want to thanks the Ocean Dynamics group at NIWA, where I conducted my research. I enjoyed working at NIWA and the experience I gained from working at a research institute. The afternoon tea breaks where we discussed anything from our research to the windy weather in Welly and the Friday night drinks at the Waitoa. I also want to thank my fellow students at NIWA, who were there for me along the way. Thanks for all the support in hard times, the little chats and board game evenings. It has made my time at NIWA so much more fun!

Last, but not least, I want to thank my husband Russell. Who is always there for me, in good times and in bad times. Not only during my thesis, but also during my bachelor and masters study. You supported me when I was stressed for a deadline or an upcoming presentation. I could not have done any of it without your support!

1 Introduction

The change in volume and temperature transport of the currents in the Tasman Sea and around New Zealand due to climate change is analysed in this thesis. An introduction to the region will be given in detail in section 1.2. The western boundary current of the South Pacific Ocean is located Tasman Sea east of Australia and west of New Zealand and dominates the flows that transport heat and biota from tropical waters in the north into the Tasman Sea [Godfrey et al., 1980]. The East Australian Current (EAC) flows poleward along the east coast of Australia where it enters the Tasman Sea. After the separation at around 32°S, it splits into an eastward current towards New Zealand, called the Tasman Front (TF) and a southward current that continues along the coast towards Tasmania [Oke et al., 2019]. A coarse fraction of the southward EAC extension exits the Tasman Sea here through the Tasman Leakage (TL) [van Sebille et al., 2012].
Western boundary current regions are identified as hot-spots for above average warming and intensifying marine heat waves [Oliver et al., 2014]. In the past decades, temperatures at the surface and subsurface of western side of the Tasman Sea have warmed at a rate 3-4 times the global average [K. Ridgeway, 2007].North of New Zealand, marine heat waves are projected to intensify, if the current level of emissions continues [Behrens et al., 2022]. Rising ocean temperatures and marine heat waves have a large impact on the ecosystem. Species are likely migrate away from the area if possible, or face a high rate of mortality and warmer oceans cause coral bleaching [Salinger et al., 2019] that affects the Great Barrier Reef. Increasing ocean temperatures also impact the climate. Storms will intensify, as ocean temperatures rise [K. Trenberth, 2007], which increases the likelihood for extreme weather events. It is therefore important to get a better understanding how the ocean currents around New Zealand and Australia alter due to climate change.

Several studies have been done to predict the change of western boundary currents in the future. Cai et al., [2005] found that an upward trend of the Southern Annular Mode (SAM) intensifies the subtropical gyres and causes an increasing southward extension of the EAC. Oliver et al., [2014] studied the spin-up effect of the South Pacific Gyre using a global climate model simulation, and found that the transports along the EAC and EAC-extension is projected to increase. Sen Gupta et al., [2021] studied the effect of a high emission scenario on western boundary currents across the globe. They found that the East Australian Current core flow, before it diverges, shows little change. The volume transport continuing south in the EAC-extension towards Tasmania increases, while the volume transport towards New Zealand is predicted to decrease in the high emission scenario. The temperature transport between the EAC and New Zealand has not been studied before in detail. Marine heatwaves are projected to become more frequent and increase in strength in the future in the region north of New Zealand, if current emissions of green house gasses continue [Behrens et al., 2022]. This contradiction between a decrease in volume transport of the subtropical waters towards New Zealand and the intensifying marine heat waves in that region, motivates the question to what extend the temperature transport towards the New Zealand is altered by climate change and how other regions in the Tasman Sea are affected by the change in transport.

1.1 Background and research question

The prediction of decreasing volume transport in the Tasman Front (TF) and the intensification of marine heat waves north of New Zealand is the motivation to study the change in volume and temperature transport throughout the Tasman Sea. This report studies the oceanic temperature transport in the region that can help to get a better understanding of the change in strength, frequency and location of marine heat waves.
The change in volume transport and temperature transport will be studied with an Eulerian and Lagrangian analysis. The zonal mean of the wind stress curl of the westerly winds will be correlated to the transports to identify the driver of the change in current strength.
The change in volume transport in the EAC has been studied before [Oliver et al., 2014], [Sen Gupta et al., 2021]. But little is yet known about the temperature transport in the region. We expect to observe a similar trend in the change of volume transports in the western boundary current system, as Sen Gupta et al., [2021]: a decrease in volume transport towards New Zealand and an increase towards the Tasman Leakage. The ocean heat content has a causal link to the intensity of marine heat waves [Behrens, et al., 2019]. Which means an increase in temperature transport towards New Zealand could be a driver of the intensification of marine heat waves in the region. We therefore expect an increase of temperature transport towards New Zealand, despite the projected decrease in volume transport. The use of a high resolution model that is eddy permitting and able to resolve mesoscale activity, allows us to study the currents in the region in more detail. A Lagrangian analysis is used to study the connectivity between the EAC and the other regions in the Tasman Sea. As the EAC is the main oceanic source of heat into the Tasman Sea, this can help us understand to what extend the warm subtropical waters increase local ocean warming that fuel marine heat waves.

1.2 Tasman Sea

The Tasman Sea is located between Australia and New Zealand. The Western Boundary current of the South Pacific ocean gyre [Matear et al., 2013] is called the East Australian Current (EAC) and enters the Tasman Sea along the East coast of Australia as it flows poleward. It transports warm subtropical waters into the Tasman Sea [Behrens et al., 2020], that support marine life and ecosystems and influences the weather and climate of Australia and New Zealand [Oke et al., 2019]. An overview of the EAC system is shown in Figure 1.The EAC core flow bifurcates at approximately 32°S [Oke et al., 2019] in a complex eddy-field [Chiswell et al., 2015]. The surface-intensified flow is called the Tasman Front (TF) and crosses the Tasman Sea towards New Zealand. The part of the EAC that continues along the Australian coast as an eddy-rich southward flow called the EAC-extension (EAC-ext) [Godfrey et al., 1980]. At approximately 46°, a coarse fraction of the EAC-ext exits the Tasman Sea through the TL, while a small part recirculates back into the Tasman Sea. The southern boundary of the Tasman Sea is identified by the Subtropical Front (STF), that is theoretically located between the positive wind stress curl in the subtropical region and the negative wind stress curl in the subantarctic region at a latitude of zero wind stress curl. It separates the cooler subantarctic waters with the warmer subtropical waters [Munk and Carrier, 1950]. Between Tasmania and the South Island of New Zealand, the mean latitude of the STF is approximately 46°S [Behrens et al., 2021]. The TF continues eastward along the coast of New Zealand's North Island as the East Auckland Current (EAUC), and turns

southward as the East Cape Current [Chiswell et al., 2006]. When it reaches the Chatham Rise, it turns to an eastward flow where it mixes with subantarctic waters [Roemmich and Sutton, 1998]. The Southland Current (SC) start at the southern point of New Zealand off the coast of Stewart Island [Sutton et al., 2003] and flows northward. Which is unique as it is an equatorward moving western boundary current. Westerly winds induce a northward Ekman transport, that enables overshoots of the ACC to flow northward in the region of the eastern continental shelf and feed into the SC. These currents south of the Chatham Rise are influenced by the bathymetry of the Campbell plateau, Bounty Trough and Chatham Rise as is visible in Figure 2. In this region the STF is pushed northward, it follows the SC along the east coast of the South Island of New Zealand and turns eastward as it reaches the southern boundary of the Chatham rise [P. Sutton, 2001]. Figure 2 also gives a representation of the water masses and other fronts in the region of the Tasman Sea. The northern region of the Tasman Sea is warmer, due to the inflow of subtropical waters in the EAC and the southern region of the Tasman Sea is cooler, due to the mixing with subantarctic waters [Chiswell et al., 2015].

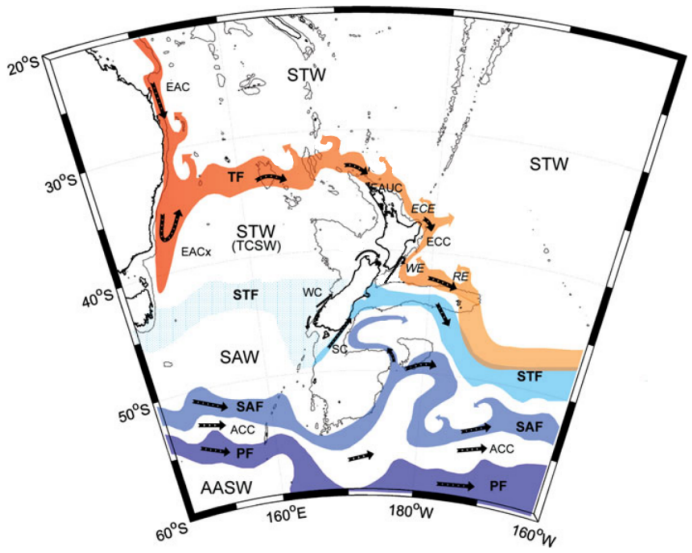

Figure 2: The currents southeast of New Zealand are, beside the wind stress, also influenced by the bathymetry. The SC originates at the south eastern point of New Zealand, the fraction of the Sub Antarctic Front (SAF) branches off, moves northward and feeds into the SC. The Chatham Rise obstructs the current from moving further north, the coarse part of the SC turns eastward before it re-enters the South Pacific basin. This image also shows the location of the subtropical water (STW), the subantarctic water (SAW), the location of the subtropical front (STF) and Tasman Front (TF), subantarcit front (SAF) and the Polar Front (PF). The color scheme represents the temperature of the Current, where red is the warmest flow, and dark blue the coldest. The East Australian Current (EAC) transports warm subtropical water (red) into the Tasman Sea and further south in the EAC-extension. The subtropical waters flow towards New Zealand in the TF (orange) and past New Zealands North Island in the East Auckland Current (EAUC), East Cape Current (ECC) and out into the South Pacific basin. The permanent eddies, East Cape Eddie (ECE), Wairarapa Eddy (WE) and Rekohu Eddy (RE) are displayed as well. South of the Antarctic Circumpolar Current (ACC) is the cold Antarctic Surface water (AASW) An Edited image from [Chiswell et al., 2015].

2 Theory & method

2.1 Wind driven theory

Wind is a dominant driver for ocean surface currents and the large scale ocean circulation. A change in strength and location of the wind speed, therefore, influences the strength of the currents. The Westerly winds are projected to change due to a positive trend in the Southern Annual Mode (SAM) [Cai et al., 2005]. The strengthening or change in location affects the wind driven circulation in the subtropical gyre. This causes a spin-up effect in the western boundary current of the South Pacific wind driven ocean circulation, that causes the EAC to penetrate further south, as was also confirmed by Oliver et al., [2014] and Sen Gupta et al., [2021].
Large scale ocean circulation is driven by Ekman transport [V. Ekman, 1905] and the underlying theory is explained in this section. A broad weak surface flow transports water equator ward. This water is transported back poleward in a narrow and strong flowing current. The conservation of vorticity requires the poleward transport to be on the western side of the ocean basin. In the Southern Hemisphere, the relative vorticity of the water parcels is increased by the wind shear as is moves equatorward. The friction caused by a flow along the western boundary of the ocean basin reduce the relative vorticity while the friction of an eastern boundary would increase the vorticity even further [Marsh and van Sebille, 2021]. The Coriolis force shifts the centre of the gyre westward, and narrows and intensifies the poleward transport, creating these strong western boundary currents. Changes in basin-wide wind stress, affects the wind driven ocean circulation and the strength of the flow in the western boundary current.
This section explains the underlying mechanism of the wind driven ocean circulation and how this affects the western boundary current.

The friction between the wind speed and ocean sets the ocean in motion. The force that generates the motion is balanced between the shear stresses and the Coriolis force [V. Ekman, 1905].
The theory can be explained by treating the ocean as different layers that can move independently. The shear stress on one ocean layer is caused by the difference in speed of the layer above and below it, which is the wind speed for the surface layer and the ocean speed in the layer above it for any layers below the surface. The energy of the induced motion transfers downward into the ocean from layer to layer and the speed of the induced motion decreases with depth as energy is lost in each transfer. The Coriolis effect diverts each layer with respect to the layer above it, resulting in the Ekman spiral which the penetrates downward into the ocean until the energy of the shear stress is dissipated. A net flow, called Ekman transport, is generated 90° to the right of the wind direction in the Northern Hemisphere and to the left in the Southern hemisphere. The velocities of the Ekman transport can be calculated with

$$\begin{aligned} U &= \frac{\tau_{ys}}{\rho f} \\ V &= -\frac{\tau_{xs}}{\rho f}. \end{aligned} \tag{1}$$

τ_{xs} and τ_{ys} are the wind stress in zonal or meridional direction and f is the Coriolis force [Marsh and van Sebille, 2021]. The Coriolis force changes over latitude, it is strongest at the

poles and the weakest around the equator. The gradient of the Coriolis force is defined as the β-parameter, $\frac{\partial f}{\partial y}$. East ward winds cause an Ekman transport poleward (equatorward) and westward winds an Ekman transport equatorward (poleward) in the Southern (Northern) hemisphere. The global prevailing winds are the Trade winds and the Westerly winds. The Trade winds are easterly winds located just north and south of the equator and the Westerlies are located at the mid-latitudes. The Coriolis force and these prevailing winds create gyres in the large ocean basins, that flow clockwise in the Northern hemisphere, and anti-clockwise in the Southern Hemisphere.
Each ocean basin has a basin-wide gyre, that is broad and weak on the eastern side of the basin and strong and narrow on the western side of the basin, called the western boundary current, like the EAC that we study in this thesis. The volume transport of the western boundary current can be calculated with the wind stress curl, the density of the ocean water and the β-parameter. This is known as the Sverdrup balance. The causal relation between the wind stress curl and the transport of the super gyre can help us predict the changes in the western boundary current system. The Sverdrup balance is defined as,

$$\beta V = \frac{curl(\tau_s)}{\rho}, \tag{2}$$

where V is the meridional velocity, τ_s the wind stress and ρ the density. This balance dictates that the vorticity loss or gain induced by the wind stress pattern is balanced with the imposed vorticity from the Coriolis gradient [Marsh and van Sebille, 2021]. V can be defined using the stream function as

$$V = \frac{\partial \psi}{\partial x}, \tag{3}$$

combining Equation 2 and 3 we obtain the streamfunction

$$\psi = \int \frac{curl(\tau_s)}{\beta \rho} dx, \tag{4}$$

that describes the motion of the super gyre. Conservation of volume transport dictates that all water that is moved equatorward has to return back to the poles. So the water that is transported equatorward due to the wind stress, returns poleward on the west side of the basin. When we combine Equation 2 and 3, and integrate both sides of Equation 4 in negative x-direction, we obtain the volume transport of the western boundary current.
The wind stress induced change in the ocean circulation therefore alters the volume transport in the western boundary current system. The projection of the poleward shift and strengthening of the Westerlies predicts that the transports through western boundary current also change as it causes a spin-up of the Gyre [Oliver et al., 2014].
The poleward shift of the Westerlies reduces the Ekman Transport in the Subantarctic waters and allows the EAC to penetrate further southward. A correlation between the basin wide wind stress and the volume transport in each of the current allows to quantify this relation to determine if the basin wide wind is a main driver of the change in the EAC system.

2.2 Shared Socioeconomic Pathways

The model that we use simulates three different climate pathways based on the CO_2 concentration in the atmosphere. Those climate scenarios are defined by the Shared Socioeconomic pathways

(SSPs). They are developed by the UN to study the impact of climate on society and predict which challenges humanity might have to face in the future, based on their emissions of green house gases. They describe the social, economic and natural challenges society will likely have to face if it follows a certain emission scenario [O'Neill et al., 2013]. The UN defined the characteristics of 5 different climate pathways. The three climate scenarios simulated in NZESM are SSP1-2.6, SSP2-4.5 and SSP3-7.0. The second number in the pathway name represents the radiative forcing due to the CO_2 concentration in 2100. The pathway itself is defined by the by CO_2 concentrations in the atmosphere. We will refer to those pathways in the rest of this thesis as SSP1, SSP2 and SSP3.
SSP1 represents the low-emission scenario, that requires a large shift to renewable energy sources and a strong reduction in emissions. SSP3 the high emission scenario, where humanity will continue to rely mainly on fossil fuels. SSP2 is the middle road, this scenario assumes humanity will shift slowly to renewable energy, and still relies on fossil fuels for the first part of the century.
The outcome of SSPs are used for policy making, mitigation and adaptation and can help persuade governments to cut back emissions so those challenges don't have to be faced in the future.

2.3 The model

The model used in this study is New Zealand's Earth System model (NZESM) [Behrens et al., 2020]. It is based on the UK Earth System Model (UKESM) [Kuhlbrodt et al., 2018], but distinguishes itself by having a two-way high resolution nested area in the region around New Zealand and the Tasman Sea. The UKESM has a 1° nominal resolution, while the nested area has a resolution of 1/5° and spans from 132.7°E-143.7°W and 60.17°S-10.75°S [Behrens et al., 2020]. This results in grid sizes within the nested area of 12-20km and allows to resolve meso-scale eddy activity. For this reason, there is no eddy parameterization applied within the model. The vertical grid contains 75 levels, which are 1m near the surface and increases with depth to 200m. The advection data and many other variables like temperature and salinity, and wind stress are stored on an Awakara C-grid as 5-daily averages. It does not contain the vertical velocities, but these can be computed using the continuity equation.
NZESM is a fully coupled earth system model, which means it combines model components to simulate the ocean physics (NEMO) [Madec et al., 2017], the atmosphere (Unified Model) [Walters et al., 2019], cryosphere including sea-ice (CICE) [Rae et al., 2015], [Hunke et al., 2017], land surface (JULES) [Walters et al., 2019], ocean biochemistry (MEDUSA) [Yool et al., 2013]. However, within the nested high-resolution domain only the physical parameters are simulated on the high resolution grid. The physics and biochemistry are simulated with the coarser model at 1° resolution, but due to the coupling the model they will be affected by the increased resolution.
The model simulation of UKESM starts after a spin-up state called "start dump" in 1850. CO_2 is added to the atmosphere to simulate the industrial revolution. This spin-up state in 1950 is used to initiate NZESM. The simulation continues creating the historical simulation. A technical aspect of the construction of the nested area, is making sure the model does not lead to instability when the high-resolution area is added and accounts for a potential spin-up effect of the new resolved mesoscale activity. The model continues to simulate the

additional CO_2 emissions in the atmosphere in the historical simulation until 2014. At this point, the simulation diverts into three different emission scenarios: a low emission scenario (SSP1), a high emission scenario (SSP3) and a middle road scenario (SSP2) [O'Neill et al., 2013]. These climate scenarios will be described in paragraph 2.2 in more detail. The CO_2 concentration in each of the climate pathways correspond to their anthropological emission projections.
The high resolution of the nested area within NZESM is able to resolve mesoscale activity. Because anticyclonic eddies play an important role in the separation of the EAC [Ypma et al., 2015], this embedded high resolution nested area enables to get a better understanding of the transports in the current system in the Tasman Sea and around New Zealand.

2.3.1 Model Validation

The NZESM model is validated in Behrens et al., [2020]. The output of the simulations is compared to the UKESM and data of EN4, which is the 4^{th} version of a quality controlled ocean temperature and salinity profile data set of the Met Office Hadley Centre [Good et al., 2013]. As part of this master thesis research, NZESM is verified by comparing the Eulerian volume transports of cross sections shown in Figure 3 with findings of other studies and with another available hindcast model: NZ20 [Behrens et al., 2021]. The exact locations of the cross sections are displayed in Table 1. The computational method of the Eulerian volume transports will be explained in paragraph 2.4. Tools used in the studies to validate NZESM, are for example models, altimetry data and ocean observations made by drifters and buoys. The NZ20 model is an ocean model on a $1/4°$ horizontal eORCA grid with a high-resolution nested area of $1/20°$ in the same region as the nested area in NZESM [Behrens, et al., 2019]. Due to its high resolution, it is able to fully resolve mesoscale activity and partially able to resolve sub-mesoscale activity.

	longitude [°E]	latitude [°S]
EAC	153-156	30
TF	173	30-34.4
TL	146.6	43.5-48
ECC	178.3-182	38
SC	169.5-172.7	46.5
CS	174.1-175.1	42.3

Table 1: The exact location of the cross sections used of the analysis is displayed in this table. These locations are chosen based on previous studies, to allow comparing the volume transport calculated with NZESM with the literature values.

2.4 Analysis

In this study an Eulerian and Lagrangian analysis are performed using NZESM. The Eulerian analysis is used to validate the model against other studies and to get an initial idea of the representation of the currents in NZESM.

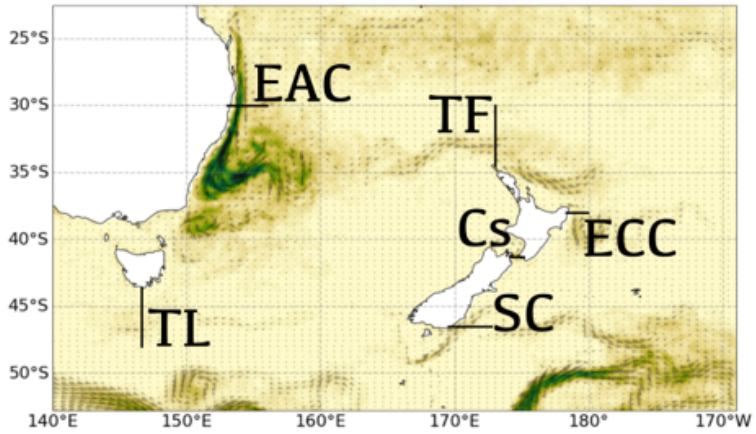

Figure 3: The cross sections that are examined in this study and used to verify the model are shown here. The main cross sections are the EAC, TF and the TL. The background flow is the mean velocity of the top 500m, which visualises the motivation of the cross section locations and confirms that the main flow into the Tasman Sea, represented by the dark green area off the east coast of Australia, is through the EAC.

The Lagrangian analysis enables us to study the connectivity between regions, as we are interested in the temperature transport between the EAC and the region North of New Zealand. The method is executed with OceanParcels, a model in Python, that will be explained later in this section. The difference between heat transport and Temperature transport is explained later in this section.

Eulerian analysis
The data from NZESM is located on an Arakawa C-grid. The initial analysis in this thesis is an Eulerian analysis of the volume transports of the cross sections shown in figure 3. The Eulerian cross sections are used to validate the model as explained in section .
The mean volume transport of the top 2000m of each cross section is calculated over time, in the historical simulation between 1995-2014 and the future period from 2050-2100. The intensity of the current is defined by calculating the sum of the volume transport of the top 2000 meters of the current from the coast outward into sea to the ocean side of the cross section. Only the top 2000 meters the current is used to calculate the sum, because the contour plots showed that below this depth a recirculation is present in the EAC and the TL. As we want to study the change in the core of each current and not the recirculation, this would not give an accurate representation of the intensity of the current. The depth at other cross sections are not greater than 2000m. The sum from the coast outward can calculate the intensity of the current while taking the zonal (or meridional) variability of the current over time into account. It also allows us to study the change in width of the current for each of the future scenarios.

Lagrangian analysis
The main technique used in this research, is the application of a Lagrangian analysis of the western boundary current system in the Tasman Sea. This analysis is performed with OceanParcels, which is a set of python classes that simulate the Lagrangian transport in the ocean [van Sebille et al., 2018].

In a Lagrangian analysis, virtual particles or parcels are seeded in a velocity field. These parcels represent a volume transport and are able to track the passive transport of for example organisms, plastic or other tracers in the ocean. The connectivity between regions can be studied as the volume transport can be attached to each ocean parcel and analysed at the cross sections. The volume transport along the trajectory of the parcel is constant, as NZESM is a Boussinesq fluid. The concentration of tracers within a fluid parcels are however not conserved, due to inter grid cell gradients. The tracer material within an ocean parcel at a certain time, is not necessarily the same tracer within that parcel at a later time step. An intuitive way of thinking about ocean parcel, is looking at it as a (small) volume in the ocean. But fundamentally, it represents a bundle of volume stream lines, called a stream tube [van Sebille et al., 2018].
The law of conservation of mass, dictates that the volume transport along streamlines is conserved. A streamtube is a bundle of stream lines, where the sides of the streamtube are parallel to the velocity. Transport in the ocean and ocean models can be represented by streamtubes, as we consider the ocean to be incompressible and therefore has a non-divergent velocity field, $\nabla \cdot v = 0$. As a streamline is equivalent to a material pathway, a streamtube is a material tube in a piecewise steady-state flow and volume transport is conserved along its trajectory. If we integrate the non-divergence property at each end of a streamtube in the ocean, with Gauss's Law, the conservation of volume transport can be shown.

$$\int_{A_1} \vec{v} \cdot \hat{n} dA + \int_{A_2} \vec{v} \cdot \hat{n} dA = 0 \tag{5}$$

Within the Lagrangian analysis, a streamtube is represented by a single ocean parcel. Based on the conservation of mass and Equation 5, the volume transport at the cross sections is equal to the volume transport at the seeding location.
The Lagrangian simulation computes a trajectory of each parcel that is seeded based on the position vector in space and time, a continuous velocity field and the Runge-Kutta methods. The continuous velocity field is computed by interpolating the Eulerian velocity field and is executed with a package within OceanParcels, called field set. These packages can transform velocities on the most common Eulerian grid types, like the Arakawa A-, B- or C-grid to a continuous velocity field. The interpolation also takes boundaries, like the coastlines and bathymetry, within the model into account, to prevent any parcels ending up on land which then get stuck. It is possible to compute a continuous velocity field of any grid type with one of the field set packages yourself, but this a difficult procedure. These field set packages are therefore very useful, and it is important to apply the right field set function with the corresponding grid, to prevent stuck particles.
The advection of a parcel can be calculated with numeric methods, based on the velocity field. The most common method used in OceanParcels is the 4^{th} order Runge-Kutta integration scheme. The new location of the parcel is calculated at each time step based on the velocity field and its current position. The position of the parcels are exported into a data set, which allows the analysis of the trajectories. In this research, the Runge-Kutta scheme time step is 1 hour and the positions of the parcels are exported every 5 days, equal to the temporal resolution of the Eulerian field.

Difference between heat transport and temperature transport
The volume along trajectories is conserved, as explained earlier. But mixing of tracers and temperature between stream tubes is possible. Heat transport is defined based on a net-

zero mass flux [van Sebille et al., 2012], for example over a cross section that spans from the western to the eastern boundary of an ocean basin. The heat transport calculated with Lagrangian trajectories, would require the particles to re-enter the Tasman Sea to obtain a net-zero mass flux. This would need 1000's of year of simulation if they re-enter at all. The distribution of heat that is being transported into the Tasman Sea by the EAC towards the regions around New Zealand and Australia can be expressed with temperature transport [W] defined as

$$H_T = \int \rho c_p T v dA, , \tag{6}$$

where T is the temperature in °C of the ocean parcel at a given time, ρ the density of ocean water, which is assumed constant in this research at 1025 $^{kg}/_{m^3}$ and c_p is the specific heat at 3900 $^{J}/_{Kg°C}$.

Simulations

Parcels are seeded in the East Australian Current cross section from 1950-2014 in the historical simulation and from 2030-2100 in the future simulation. A continuous seeding strategy is applied; a new set of parcels are released after a set time interval. In this study the time interval between seeding is same as the interval between data sets, which is 5 days. The seeding cross section is located between 152-156°E up to 2000m. A single parcel is seeded in each grid cell with a southward velocity, as the main direction of the EAC is southwards. The Eulerian data set only contains the zonal and meridional velocity, the vertical velocities have been computed afterwards using the continuity equation. Two sensitivity simulations are performed in the historical period, to study the effect of including the vertical velocities. One simulation is performed with only the zonal and meridional velocities and one that also includes the vertical velocities. The movement of the parcels is made visible in an animation, which can be found in the link in Appendix A.1. It shows that when only the horizontal velocities are used, relatively more parcels get stuck at the coast because convergence at the coast is not represented in the simulation without vertical velocities. Hence, the simulations used in this study are performed using the zonal, meridional and vertical velocities.

The year in which the simulations start is chosen based on the available data. The simulation in the historical period starts in 1950 until 2014. The simulations in the future scenarios start in 2030 and finish in 2100, so both simulations span over a similar length of time.

In the simulation it is possible that the parcel recirculated and crosses the seeding location in the EAC. These parcels are deleted as soon as they cross the seeding location in the simulation, because a parcel is described by a larger spacial area, in this case the seeding grid cell, and timespan, the 5 day mean in the Eulerian velocity field. The continuous seeding method requires to delete this parcel to comply with the conservation of volume. When a parcel crosses the seeding location during it's trajectory, and a new parcel is seeded, the volume of that parcel is already captured in the 5-daily mean of the new parcel.

The volume transport and temperature transport are attached to a parcel at the start of the simulation, so it can be analysed afterwards. The volume transport is conserved along the trajectory, but the temperature is not due to mixing. Therefore the temperature is tracked along trajectory and which allows it to compute the temperature transports at the chosen cross sections.

The volume transport V_T is defined as,

$$V_T = \int v dA, \tag{7}$$

where v is the velocity and A the area of the grid cell the parcel is seeded in. It is calculated by the depth of the grid cell times the width in longitude or latitude for a meridional and zonal flow respectively. Temperature transport is defined in Equation 6 and is calculated at each step along the trajectory as the temperature is not a constant variable. It accounts for the mixing and change in temperature between the parcels, which represent the stream tubes. The volume transport stays constant along the trajectory, hence it is only calculated at the seeding location.

Process trajectories
The information of the trajectories are stored in several variables: time, longitude, latitude and any variables that are added in the run like the volume transport and temperature. The rows in the data set represent a single parcel and each column is the data for each exported time step. The python package 'LineString' is used to determine if a parcel intersects with one of the cross sections. The volume- and temperature transport is added to the first time step the parcel crossed the cross section in the direction of main flow of the current. In the Tasman Front, this is eastward, in the Tasman Leakage, westward. If a parcel crosses the cross section a second time, its volume is not counted again. Water that recirculates over the cross section is not considered to originate from the EAC, but as regional water.
The product of the analysis is a time series of volume transport and temperature transport per cross section and a file with the information per parcel, for example the travel time between the EAC and the cross section, at which depth the parcel crosses and its volume and temperature transport. The first 20 years of this data is neglected to take the spin up effect of the Lagrangian simulation into account and is based on the travel time distribution of the parcels. These results are shown in section 3.3.

2.5 Closed box method

One parcel is seeded per grid cell with a southward velocity in the EAC cross section. To study if the amount of seeded parcels is sufficient, the percentage of parcels which exit the Tasman Sea is calculated with 50%, 60%, 70%, 80% and 90% of the parcels. If the distribution of parcels within the Tasman Seas would change by the number of parcels seeded, not enough parcels are seeded and the results of the simulation would not be reliable.
To confirm that the temporal resolution of the seeding is fine enough, a simulation is performed with a continuous seeding strategy in the historical period where parcels are seeded every 10 days instead of every 5 days. If these simulations show a different distribution over the exiting cross section, it means that the temporal resolution is not fine enough. The different simulations are compared to the control simulation, where one parcel is seeded every 5 days per grid cell in the EAC at 30 °S. The distribution is calculated in percentages for each of the simulations with the parcels that are seeded in the first 20 years of the trajectory simulation, to allow enough time for the parcels to exit the Tasman Sea. The future simulation is run for 70 years from 2030 until 2100 and the historical simulation is run 65 years from 1950-2014. This allows enough time for the parcels to exit the Tasman Sea and study the exit cross sections. The sections are as shown in Figure 4.

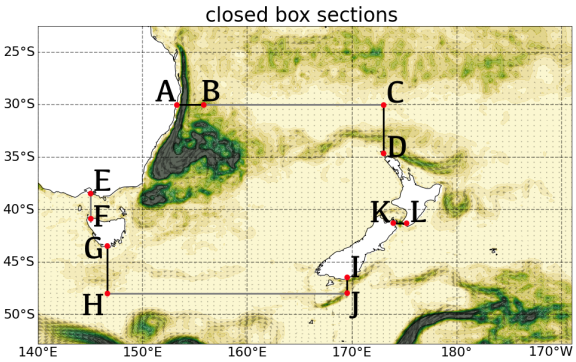

	longitude [°E]	latitude [°S]
A	153	30
B	156	30
C	173	30
D	173	34.4
E	145.1	38.3
F	145.1	41
G	146.6	43.5
H	146.6	48
I	169.5	46.6
J	169.5	48
K	174.1	42.5
l	175.1	42.5

Figure 4: The cross sections used to evaluate the exit location of the parcel out of the Tasman Sea are displayed with the black and grey lines. The location boundaries are displayed in the table.

2.6 Correlation

Wind stress is the main driver of the surface ocean circulation in the super gyre. The strength and location of the winds affects the strength of the ocean gyre and the western boundary current as explained in Section 2.1. The Westerly winds are subjected to increase in strength and move poleward, which causes a change in the western boundary current. A study from Loveday et al., [2015] concluded that the volume transport of Agulhas Current increases and is caused by the strengthening and a poleward shift of the of the Westerly winds. In the Agulhas current, the increase in volume transport broadens the current instead of intensifying the velocities.

A correlation between the strength of the Westerlies and the location of the maximum zonal mean of the Westerlies is correlated to the current strength of each of the cross section to find if the strengthening or the poleward shift of the Westerly winds are the driver of the shift in volume transport in the Tasman Sea. The global wind stress data in our model has a 1-month temporal resolution and a 1x1 degree spacial resolution. A monthly mean of the volume and temperature transport of each of the cross section is computed and correlated to the maximum value and location of the zonal mean of the wind stress.

3 Results

3.1 Eulerian analysis

The volume transport through the cross sections pictured in Figure 3 is studied for the historical simulation and the future scenarios. The mean volume transport in NZESM is calculated between 1995-2014 for the historic simulation and 2050-2100 for the future scenarios SSP1, SSP2 and SSP3. The mean in NZ20 is calculated between 1995-2014. The results are shown in Table 2 together with the literature values for these cross sections. The Eulerian velocities of the EAC, TF and TL cross sections are shown as contour plots in Figure 5. The EAC at 30°S, is a surface intensified current and extends up to 1000m depth. The maximum of the mean velocity is 0.9 $^m/_s$ in the historical simulation. In the future there is a small increase in the current near the surface between 0.1-0.2 $^m/_s$, which is visible in each of the climate scenarios. The maximum mean velocity is 0.98 $^m/_s$ in SSP1 and 1.0 $^m/_s$ in SSP2 and SSP3. The increase in velocity is visible over the total width of the current in SSP1 up to 155°E. While in SSP2 and SSP3, the increase is located closer to the coast at 154°E. The recirculation of the EAC a below 2000m shows no significant change in the future. The core of the TF current at 173°E is located just of the coast of the North Island of New Zealand and extends up to around 1100m. The largest mean velocities in the historical simulation are 0.35 $^m/_s$ and can be found the subsurface flow. In the high emission scenario SSP3, the current decreases significantly with the largest velocity anomalies between 500m and 1000m. The TF becomes a more shallow current. In the low emission scenario SSP1, the current does not show significant change. In SSP2, the current slows down between 500, and 1000m, but not as extreme as the SSP3 scenario. The maximum mean velocities in the future scenarios are 0.32 $^m/_s$, 0.24 $^m/_s$ and 0.18 $^m/_s$ for SSP1, SSP2 and SSP3 respectively. The TL south of Tasmania, flows with a maximum value of 0.1 $^m/_s$ westward and also stretches up to a 1000m depth. The largest increase of up to 0.1 $^m/_s$ is seen in SSP3 near the surface, but extends over the total depth of the current. In SSP1, the current shows a small change of less than 0.05 $^m/_s$ and increases with around 0.06 $^m/_s$ in SSP2. The bottom recirculation between 2500m and 3000m of the TL shows a small decrease of less that 0.05 $^m/_s$ over all the climate scenarios. The maximum mean velocities in the future scenarios are 0.12 $^m/_s$, 0.16 $^m/_s$ and 0.19 $^m/_s$ for SSP1, SSP2 and SSP3 respectively.

The EAC, TF and TL, show the same trend as found in Sen Gupta et al., [2021]. In the high emission scenario, the volume transport through the TF decreases and increases in the TL and little change is seen in the EAC. The width of the EAC and TL do not change significantly, and the increase in volume transport is mainly caused by an intensification of the velocities in the current as stated above. The largest decrease in the volume transport of the TF is located between 500m and 2000m, and it becomes a surface intensified, shallow current. The velocities of the future scenarios of these currents are plotted in Figure 18 in Appendix A.2. This Figure also confirms that the width of the currents do not change in the future, but are a result of increasing velocities.

The change in volume transport through the East Cape Current (ECC), Cook Strait (CS) and Southland Current (SC) are shown in Figure 17 in Appendix A.2.
The ECC reduces in volume transport in all three future scenarios, with small decrease from 30 Sv in the historical period to 22 Sv in SSP1 and a larger decrease in both SSP2 and SSP3

where the current flow at around 19 Sv. The current also becomes more narrow in SSP2 and SSP3. This is also visible in Figure 18 in Appendix A.2. This decrease in volume transport could be partially explained by the decrease in volume transport through the TF as this current turns into the ECC as it turns southward after the New Zealand's East cape. The decrease in volume transport, might be the cause of the narrowing, but this will have to be studied in more detail.
The mean strength of the CS in the historical period is just below 4 Sv. There is no significant change in SSP1 and a small decrease in SSP2 and SSP3 with the largest decrease in the SSP3. This is interesting, as the gyre is extending further southwards which could have suggested a small increase in volume transport through the CS due to the decrease in the TF.
The SC shows a very large increase in each of the future climate scenarios compared to the historical simulation. The mean volume transport in the historical period is around 2 Sv, which is much lower than the literature values based on observation of 7.2 Sv [Fernandez et al., 2018], 9.4 Sv [Sutton et al., 2003] and the model study with CMIP 6 of 11 Sv [Sen Gupta et al., 2021]. The volume transport in the future scenarios are closer to these literature values. The cause of this sharp increase in volume transport will be explained in the next paragraph.

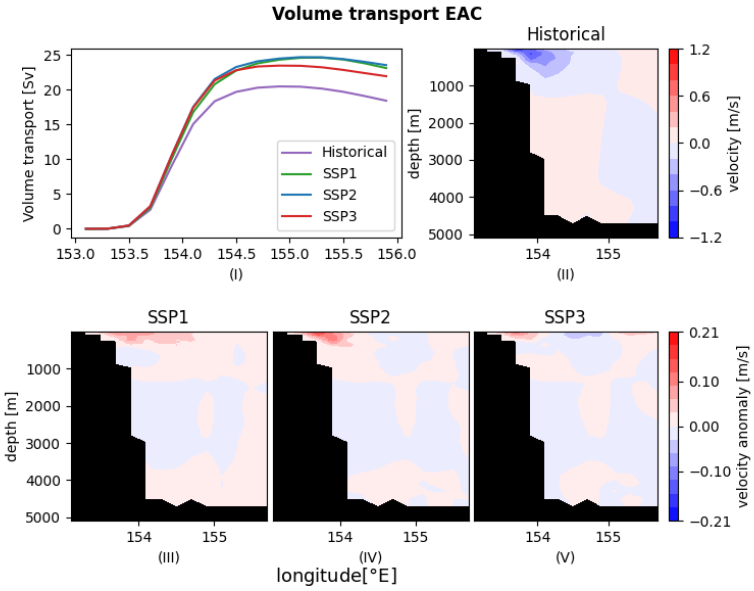

(a)

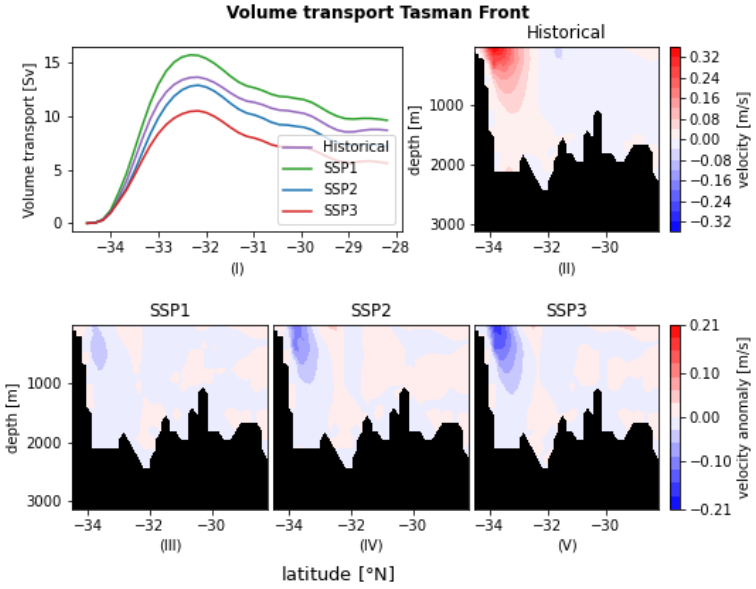

(b)

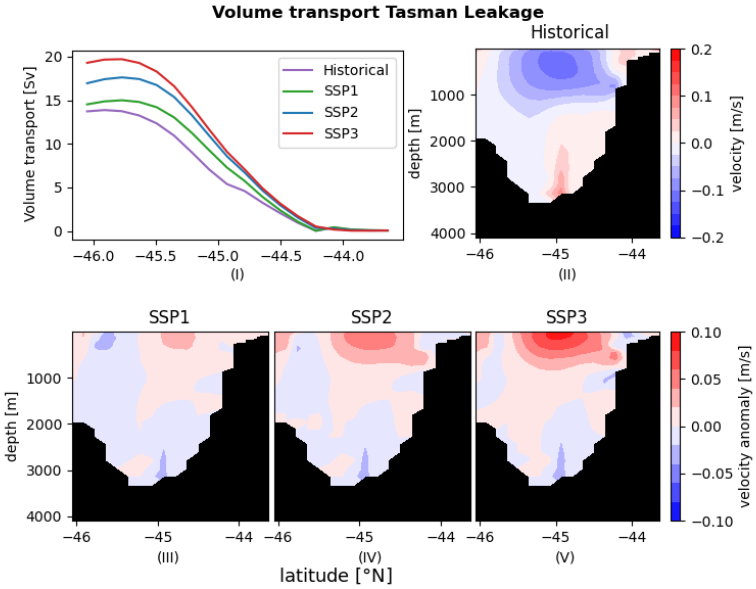

(c)

Figure 5: The Eulerian cross sections per future emission scenario. Sub-figure (I) in each of the figures is the sum of the current calculated from the coast outward. The mean velocities of the historical simulation are plotted in Sub-figure (II). The contour plots in Sub-figure (III), (IV) and (V), show the anomalies of each of the future emission scenarios compared to the reference period. Positive anomalies mean an increase in velocities and negative anomalies a decrease and they indicate the location of the largest change.

The Southland current and Subtropical front

The Eulerian initial analysis, used to verify the model, showed that the volume transports of most cross sections are in agreement with their literature values. This is not the case for the Southland current. The volume transport of the future simulations, are in agreement with

volume transport [Sv]						
Current	literature	NZ20	historic	SSP1	SSP2	SSP3
EAC	-25.2 (O) [Ridgeway et al. 2003]*	-21.8	-20.41	-24.82	-25.3	-23.73
	-27.4, -25.8, -27.5 (M) [Oliver et al., 2014]**					
	-22 (M) [Sen Gupta et al., 2021]					
TL	-8.1,-10.8 (M) [Oliver et al., 2014]	-10.7	-14.82	-15.09	-17.5	-19.8
	4.2 ± 4.3 (M) [van Sebille et al., 2012]					
	-0.9 to -4 (M) [Sen Gupta et al., 2021]					
TF	4.1,3.7,12.7 (M) [Oliver et al., 2014]	8.4	8.68	9.61	7.17	5.59
	9.7 ±5.4 (M) [Behrens et al., 2021]					
	12.9*** (O) [Ridgeway et al. 2003]					
CS	0.7 (M) [Behrens et al., 2021]	-0.6	-0.45	-0.55	-0.53	-0.51
EAUC	14.8 (O) [Fernandez et al., 2018]	9.5	9.0	11.1	8.4	7.4
	-11.8 (O) [Ridgeway et al. 2003]					
ECC	-5.6 (O) [Fernandez et al., 2018]	-7.2	-8.66	-10.08	-10.17	-10.47
	-17 (M) [Sen Gupta et al., 2021]					
	-11.6 (O) [Ridgeway et al. 2003]					
SC	9.4 (O) [Sutton et al., 2003]	14	1.81	8.53	7.7	6.85
	7.2 (O) [Fernandez et al., 2018]					
	∼11 (M) [Sen Gupta et al., 2021]					

Table 2: The volume transports, calculated with NZESM, of the cross sections pictured in Figure 3 is compared to literature values, based on models (M) and observations (O) and a hindcast model, NZ20, to validate the NZESM. The volume transports correspond well with literature values for all cross sections except the SC, which will be covered in the next section.

** EAC location 29°S*
*** EAC location 28 °S*
****TF location 168 °E*

the literature values as shown in Table 2. But the transports in the historical simulation calculated for the end of the century, were an order of magnitude smaller. Especially this significant increase was motivation to study this region in more detail. Multiple extra cross sections north and south of the first chosen cross section were examined. These cross sections all showed a lack in volume transport for both the historical simulation and future scenarios compared to literature values.

The visualisation of the velocities in the top 500m, identified the issues in this region. In Figure 6, a quiver plot of the velocity mean of the top 500m in NZESM and NZ20 are displayed. The NZ20, which has a resolution four time higher than NZESM, gives the correct representation of the current system in the region south east of New Zealand [Fernandez et al., 2018], [Sutton et al., 2003]. This suggest that a possible cause of the incorrect current system in NZESM, could be a misrepresentation in the bathymetry in the region in NZESM. As the resolution of the model could be too coarse to account for the small troughs in the bathymetry. In both models, the SC current initiates south of the coast of New Zealand's South Island and moves northward. At 46°S, the SC bifurcates in NZESM and main flow travels eastward. The first examination of the Eulerian volume transport was done just north of this bifurcation point. In NZ20, however, an overshoot of the Antarctic Circumpolar

Current (ACC) meets the SC 47°S, east of Stuwart Island, and intensifies while the SC moves northward. Another overshoot of the ACC in NZ20, re-circulates clock-wise around the Bounty plateau, preventing the SC from moving eastward. It joins the SC as it moves through the Bounty Trough before it enters the South Pacific Ocean.
The Subtropical front is the southern boundary of the Tasman Sea, and is represented by the SC east of New Zealand. The STF could therefore be shifted southward in NZESM due to the incorrect location of the SC. And the incorrect lack in volume transports in the Southland current can possibly be explained by a misrepresentation of the bathymetry of the Campbell plateau and Bounty Trough. We therefore need to be very cautious when drawing any conclusions in this region.

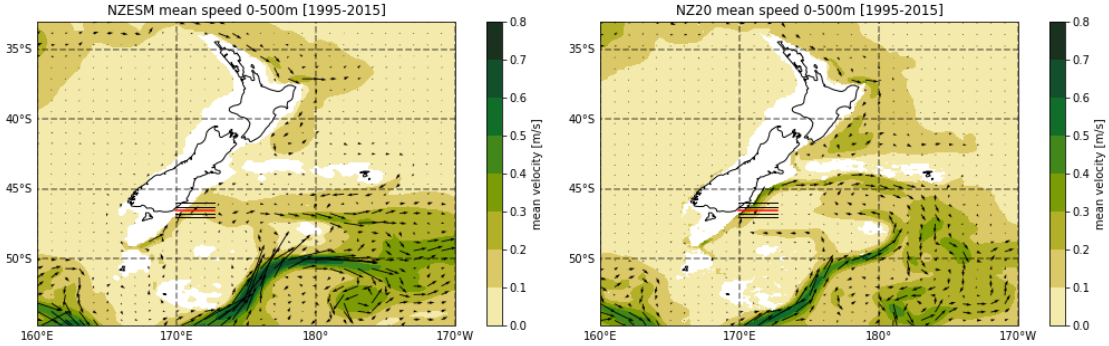

Figure 6: The mean speeds of the top 500m of the NZESM model is shown in the left graph and NZ20 in the right. The white patches in the mean speeds are regions above 500m depth. The red line represents the cross section of the Southland current that is used to examine the volume transport. The location of the Sub Tropical Front (STF) corresponds with observations in the NZ20 model, while in the NZESM the STF is located further south and less strong. Also the re-circulation around the Bounty trough is absent in NZESM. This error can be a explained by a misrepresentation of the bathymetry in the model due to a coarse model resolution.

3.2 Closed box results

The percentage of parcels, seeded in the first 20 years, that have left the Tasman Sea after the 65-70 year simulation for the historical and future period, is stated in Table 3. The historical simulation is run for 65 years from 1950 to 2014 and the future scenario for 70 years from 2030 to 2100. The percentages of parcels through each of the exit cross sections are pictured in Figure 7. The figure with the distribution for the simulations with 50%, 60%, 70% and 90% are placed in Appendix A.3. The fraction of parcels that have not left the Tasman Sea is between 1.7 and 2% for each of the simulations and the distribution is almost identical for each of the simulations. This means that the temporal resolution of the seeding is sufficient and we seed enough particles in the simulation. We therefore are able to perform the research and obtain results that are not distorted by the amount of parcels.

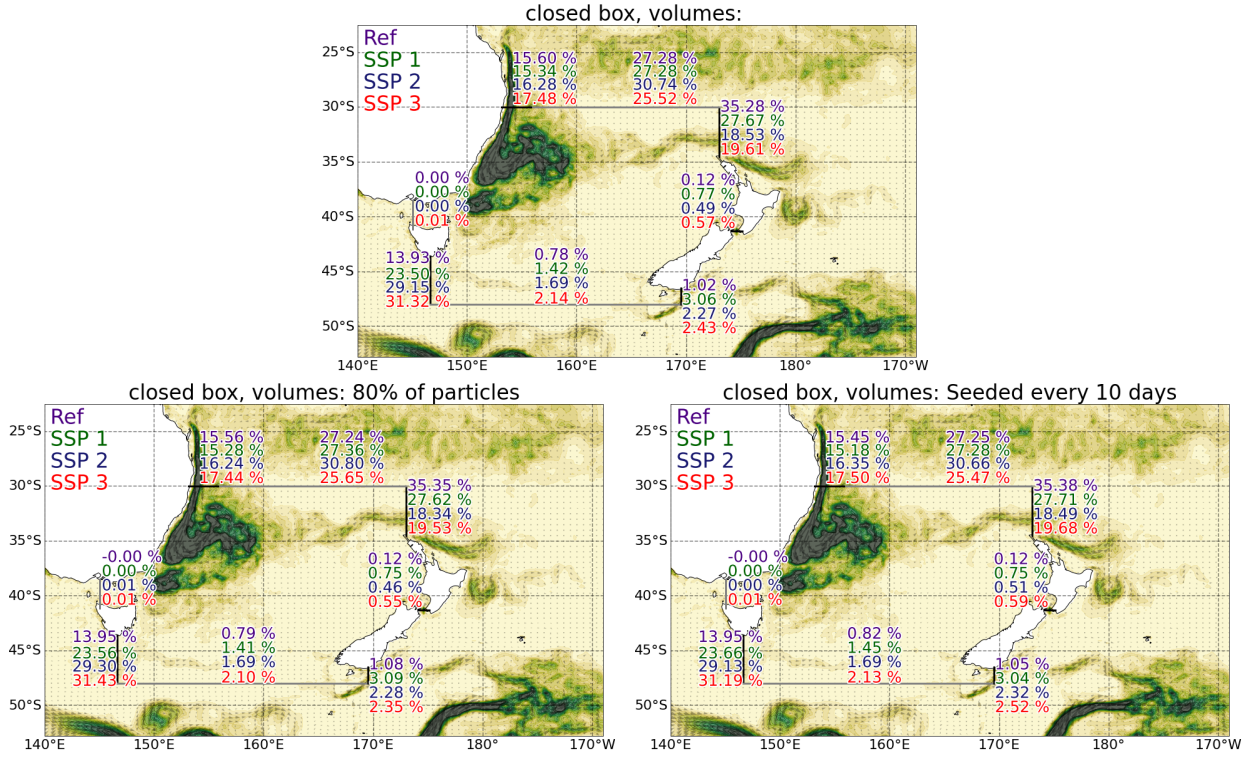

Figure 7: The percentage of the volumes carried by parcels seeded in the first 20 years of the simulations are shown for each of the exit cross sections. The purple values respond with the historical period, the SSP1 is shown in green, SSP2 in blue and SSP3 in red. The northern and southern boundary are shown in grey, to clarify the different cross sections. The contour plot in the background are the mean speeds of the top 500 meters of the ocean with a quiver plot of the mean surface speeds.

3.3 Lagrangian analysis

Time series

The volume transport and the trend through the TF and TL are shown in Figure 8. The trends in the future scenarios correspond with the expectations, a larger increasing upward trend for the TL for the higher emission scenarios and a decreasing trend for the TF in SSP3. The time series of the ECC, CS and SC are shown in Appendix A.4. The volume transport through the ECC shows the same tendency as the TF, a larger decrease in the the high emission scenario and a smaller decrease in the low emission scenario. And it therefore also follows the Eulerian trend through this cross section. The CS does not show a large increase or decrease. Interesting to note is that the mean Lagrangian transports are a factor 5-10 times smaller than the Eulerian transports. Which would suggest that there is no strong connectivity between the EAC and the CS. The volume transports through the SC show a small increase over the three climate scenarios, but stay fairly constant over the time series. The increase is likely a cause of the incorrect representation of the currents within the region, as seen in the Eulerian means. We can therefore not make any conclusions on how the current alters in the future based on these Lagrangian timeseries.

To account for the interdecadal variations within the current, the mean is calculated over 50 years between 2050 and 2100, so the simulation of the climate scenarios have had time

Fraction of particles			
	Random	Temporal	closed box
Historical	98.29%	98.28%	98.3%
SSP1	98.18%	98.21%	98.19%
SSP2	98.29%	98.28%	98.3%
SSP3	98.07%	98.11%	98.11%

Table 3: The percentage of particles and volumes that has left the Tasman Sea after 70 years of simulation time is given in this figure for each simulation type. Around 1-2% of parcels is still in the Tasman Sea after this time. Those parcels could be stuck at a coast line, moved to the ocean surface and exited the domain or still move around in eddy fields.

to diverge and the differences between the scenarios can be analysed. The mean Lagrangian temperature and volume transport through the TF and TL are stated in Table 4 and 5, together with the relative difference in transport between the future scenarios and the historical period and the relative difference between the higher emission scenarios SSP2 and SSP3 and the low emission scenario SSP1. The TF shows a decrease in volume transport in the SSP2 and SSP3, while the temperature transport shows a small increase in SSP2. The temperature transport shows a relative larger change over all cross sections and scenarios compared to the volume transport. Compared to the low emission scenario, the transport is decreasing through the TF and increasing through the TL.
A 5-year mean of the volume and temperature transport is calculated, to get a better picture of the trend without the yearly and seasonal variation, as pictured in Figure 9. There is a strong coupling visible between the volume transport and the temperature transport. The trend of the current still shows the shift in transport from the TF to the TL in the high emission scenario. The transport in SSP1 and SSP2 seem to converge towards each other for both the TF and TL. The transport through the ECC decreases for all future scenarios, but shows a larger decrease in SSP3, which is similar to the trend in the TF. The volume transport through CS and SC seems to increase significantly compared to the historical simulation. These timeseries are shown in Figure 21 in Appendix A.4. The mean volume transport through CS varies between 0 and 2 Sv, so the relative change in percentages might give a distorted image. The mean transport through the SC is around 2 Sv and shows large variability in time, which could also be caused by the misrepresentation of the current in the Eulerian velocity field.

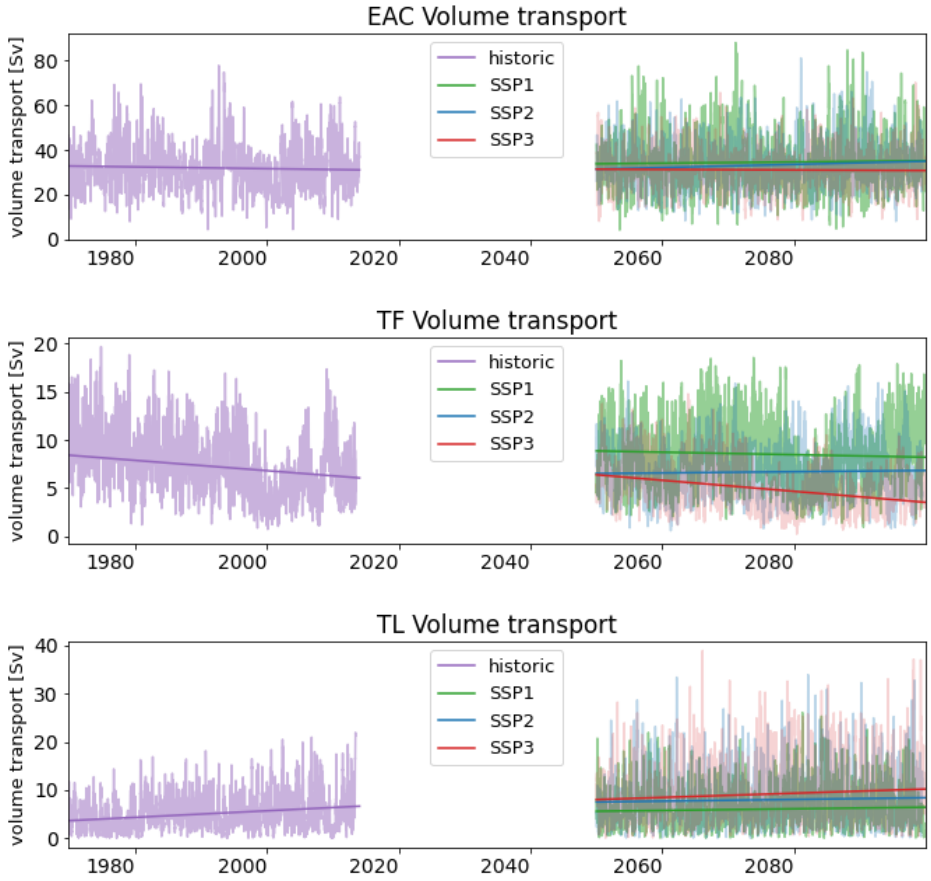

Figure 8: The volume transport of the Lagrangian transports through the TF and TL is displayed for the historical period from 1970-2014 and the future climate scenarios from 2050-2100 including the trend of each period. The data between 2014 and 2050 is left out due to the spin-up effect of the simulation. Each scenario shows interdecadal variation. In the TF, there is a decreasing trend in the volume transport, while the volume transport in SSP1 is rather constant. The TL shows a slight upward trend in all three scenarios, with a more extreme increase in the SSP3.

Travel time

The travel time is defined as the time it takes for a parcel to travel from the EAC seeding location to one of the defined cross sections. A histogram of the travel time to the Tasman Front and Tasman Leakage, are shown in Figure 10. Table 6 states the time it takes for 95% of the parcels to have crossed the section and the mean of the travel times. In the calculations, the first 20 years are discarded to account for any spin up effect of the Lagrangian simulation. The mean travel time through the TF increases, but 95% of the parcels still arrive within approximately 7.5 years. The same signal is visible in Figure 10, the distribution widens in the future pathways compared to the historical simulation. There is no clear dependency of the climate scenario on the travel time in the future for the transport through the TF. The Travel time towards the TL is decreasing, this is visible in the mean travel time as well in the time needed for 95% of the parcels to have passed the cross section. The higher emission scenarios SSP2 and SSP3, have a shorter travel time compared to the low emission scenario SSP1 and the historical simulation.

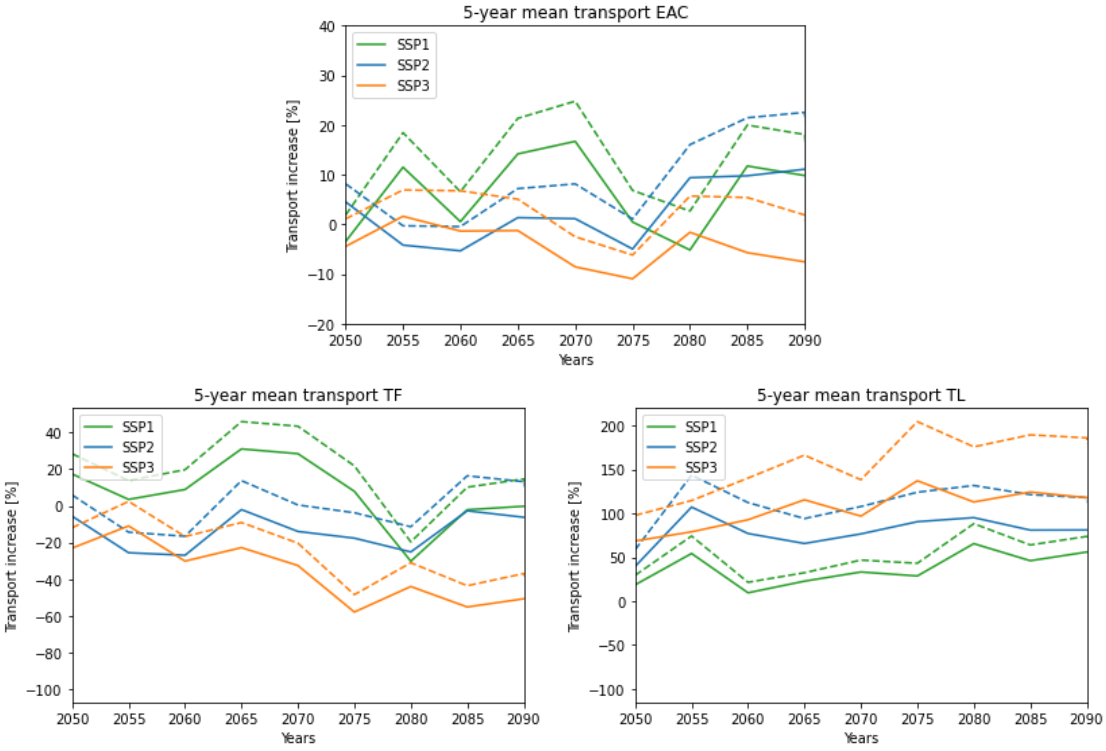

Figure 9: The 5-year mean of the volume and temperature transport anomaly through the TF and TL are given compared to the historical mean to show the trend and the interdecadal variation of the current. The temperature transport and volume transport are highly correlated. A more extreme shift in transport from the TF to the TL is visible in SSP3, while in the low emission scenario this shift is less apparent. The EAC shows no significant trend, except the decadal variation.

As parcels are seeded in EAC and start moving through the Tasman Sea, it takes time to arrive at the cross sections and produce a continuous transport over the cross section. The longest time it takes for 95% to cross the studied cross sections is 20 years to the TL, which is why the first 20 years is discarded. The first 20 years of the volume transport through the TL is shown in Figure 11. It clearly shows the spin-up effect of the Lagrangian simulation within the first 8 years. After that the yearly variability stays relatively constant for the spin up period.

Temperature transport				
		H_T [PW]	$\Delta H_T/H_T$ [ref]	$\Delta H_T/H_T$ [SSP1]
TF	Historical	0.44		
	SSP1	0.56	27.73%	
	SSP2	0.46	4.36%	-18.3%
	SSP3	0.35	-20.4%4	-37.71%
TL	Historical	0.18		
	SSP1	0.23	28.94%	
	SSP2	0.33	82.78%	41.76%
	SSP3	0.4	122.18%	72.31%

Table 4: The absolute temperature transport (H_T) through the TF and TL in given in PW and relative temperature transport compared to the reference period and the low emission scenario SSP1 in percentages. The temperature transport through the TF decreases in SSP3 relative to the historical simulation and decreases in SSP2 and SSP3 compared to SSP1. The temperature transport in the TL increases for all scenarios relative to the historical simulation, with a larger increase for SSP2 and SSP3.

Volume transport				
		V_T [Sv]	$\Delta V_T/V_T$ [ref] %	$\Delta V_T/V_T$ [SSP1]
TF	Historical	7.41		
	SSP1	8.53	15.1%	
	SSP2	6.66	-10.1%	-21.9%
	SSP3	4.95	-33.21%	-41.97%
TL	Historical	5.15		
	SSP1	5.98	16.12%	
	SSP2	7.93	53.84%	32.49%
	SSP3	9.09	76.3%	51.83%

Table 5: The absolute volume transport (V_T) through the TF and TL in given in Sv and relative volume transport compared to the reference period and the low emission scenario SSP1 in percentages. The volume transport through the TF decreases in SSP2 and SSP3 relative to the historical simulation with an increasing relative change for higher emission scenarios. The volume transport in the TL increases for all scenarios relative to the historical simulation, with a larger increase for SSP2 and SSP3.

Trajectory pathways

The pathways of the trajectories are made visible in heat maps. Figure 12 shows the relative change in the volume and temperature transport of the trajectory compared to the historical period in percentages. Each parcel is only counted once per grid cell, so these figures shows the pathways of the trajectory and not the residence time. In the low emission scenario, there is no transport shift from New Zealand towards Tasmania visible. There is a small shift in the middle-road SSP2 scenario from the current towards New Zealand to the region around Tasmania. The simulation of SSP3 shows a clear shift in transport, as was also seen in the Eulerian and Lagrangian time series. This figure shows that the changes in volume transport stretch over a wider region and are not completely based on the exact choice of the location of the cross section. The relative decrease in volume transport in SSP3 towards

		95% passed [years]	mean [years]
TF	Historical	7.65	2.06
	SSP1	7.82	2.57
	SSP2	7.6	2.69
	SSP3	7.44	2.62
TL	Historical	20.15	6.26
	SSP1	19.98	5.73
	SSP2	17.19	4.85
	SSP3	17.48	4.79

Table 6: The travel time of parcels from the EAC to the TF and the TL in years.

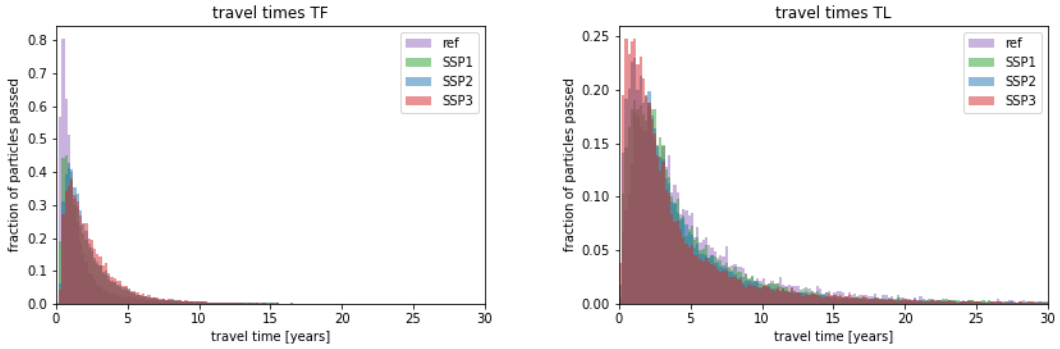

Figure 10: This histogram shows the travel time of the parcelsto the Tasman front (a), and Tasman Leakage(b). The histogram is normalised for each of the parthways. Note the different limits in the y-axis.

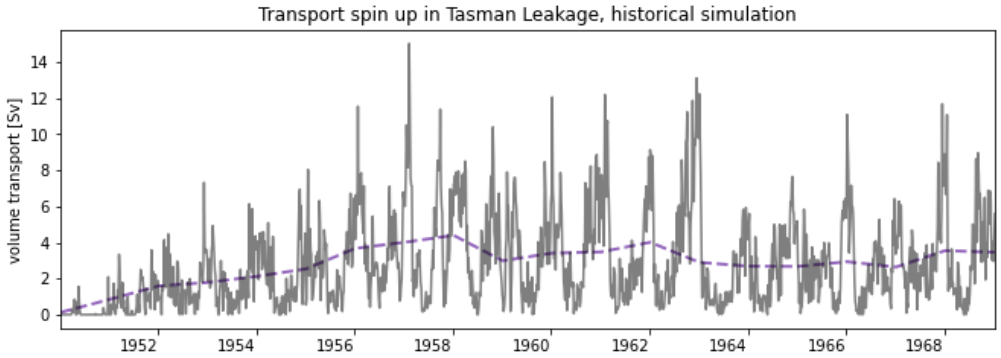

Figure 11: The spin up effect of the Lagrangian parcels is visible in the first 20 years of the transport through the TL cross section. The dark dotted line is the yearly mean of the volume transport and shows a spin up effect in the first 8 years. This is close to the mean travel time.

New Zealand is larger than the relative decrease in temperature transport. The areas with small transports, show relatively high anomalies. The CS and SC are located in these areas and need to be treated with caution.

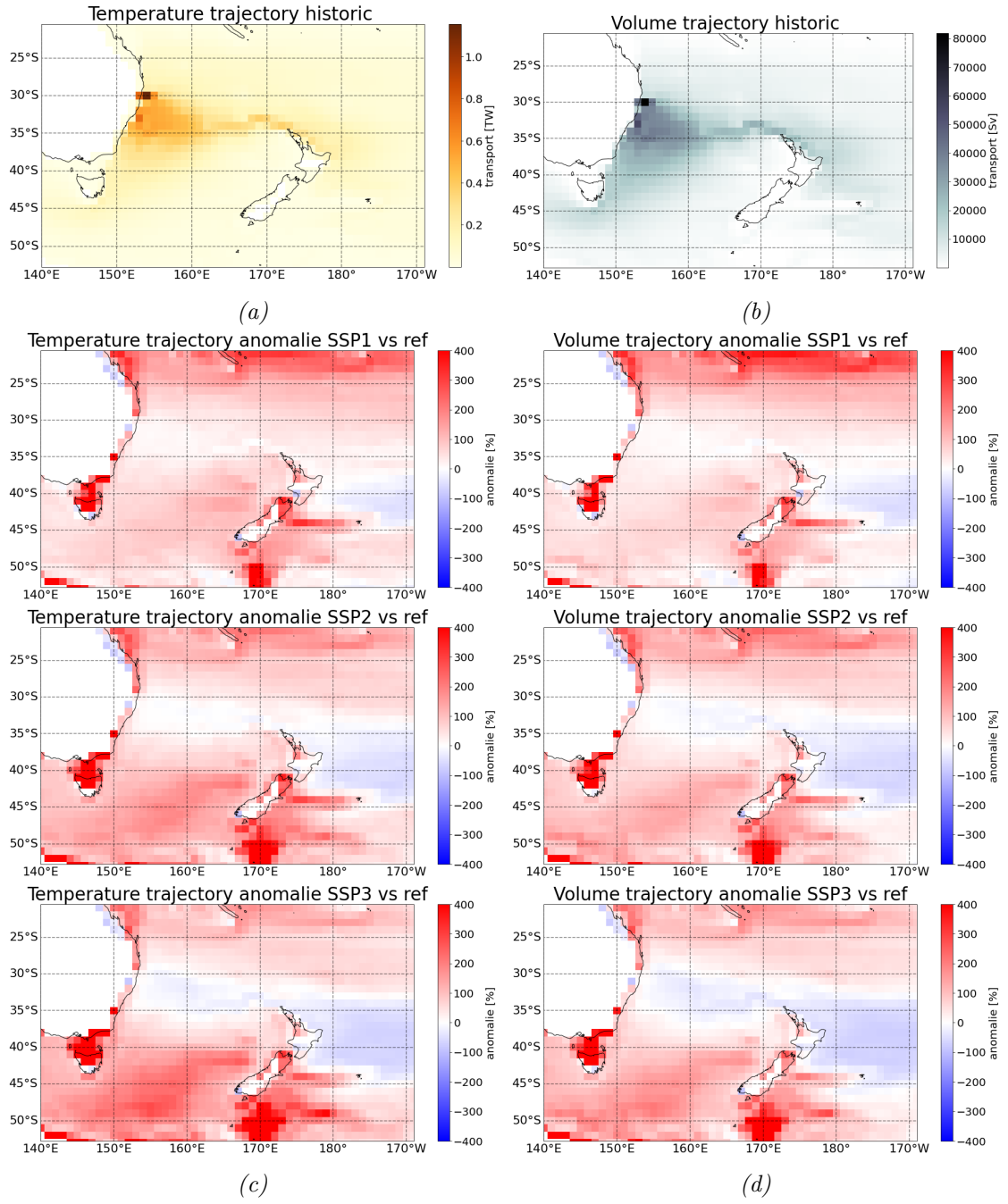

Figure 12: The volume and temperature trajectory anomalies compared to the historical period are shown in this figure. Sub figure (a), is the Temperature transport trajectory in TW an Sub figure (b) shows the volume transport trajectory in Sv for the historical simulation. The grid cell size is 1x1 degree. To visualise the trajectories, each parcel is only counted once per grid cell. Sub figure (c) shows the temperature anomaly for each of the future scenarios and Sub figure (d) the anomalies in volume transport.

Temperature along trajectory

The temperature is monitored along the trajectory for each parcel. The development of the temperature between the EAC and Tasman front is studied in this section for the different climate scenarios. The fraction of particles that are warmer that 5, 10, 15, 20 or 25 degrees are calculated for each of the emission scenarios and the historical period. In the historical period and beginning of the 21st century, there are no trajectories above 25°C. At the end of this century only a hand-full of trajectories are above 25°C. Therefore this is not shown in a graph.

There is no significant change in trajectories with a minimum temperature of 5°C and 10°C. In SSP2 and SSP3, the fraction of trajectories that are at least 15°C and 20°C, increases. This means the pathways between the EAC and New Zealand are warming in the higher emission scenarios. As shown in Figure 13, the low emission scenario SSP1, shows a relative small increase and seems to decrease by the end of the 21^{st} century. There is no obvious connection between the travel time and the fraction of warming trajectories.

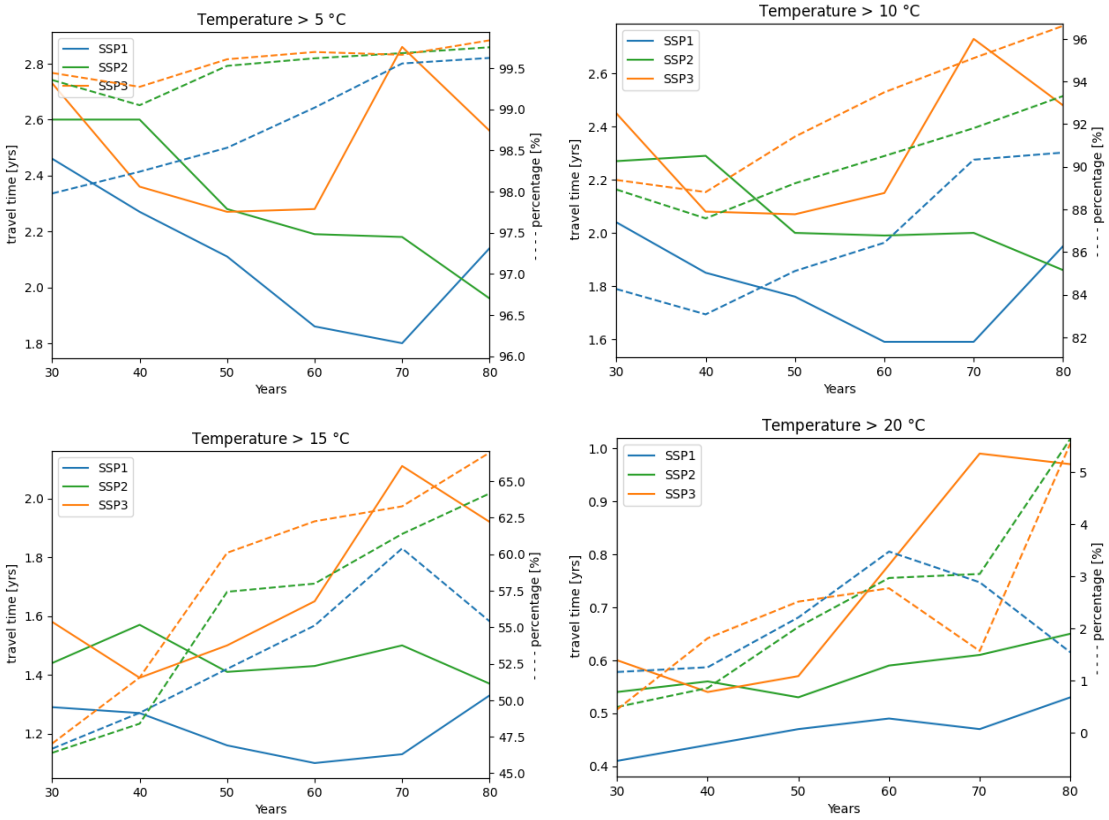

Figure 13: The 5 yearly mean of the fraction of trajectories that have a minimum temperature of 5°C, 10°C, 15°C and 20°C are shown in these figures. The solid line is the travel time in years and the dotted line the percentage of trajectories. The fraction of trajectories in SSP2 and SSP3 above 15°C and 20°C are increasing in the second half of this century. In SSP1 the trajectories fraction of warming trajectories seem to first increase around 2050-2060 and decrease again by the end of the century.

3.4 Comparison between the Eulerian and Lagrangian timeseries

The Lagrangian method allows us to tackle other questions that the Eulerian method cannot answer, for example the pathway of the ocean transport, the connectivity between regions and how properties change along their trajectory. The Lagrangian transports are often smaller than the Eulerian transports, as it only measures the parcels that are seeded in the simulation. The computer power does not allow such large simulations where Lagrangian particles are seeded at each point in the model. And seeding locations need to be chosen so research questions can be answered. In this research, parcels are only seeded in the EAC. This allows us to study the connectivity between the EAC and the other regions in the Tasman Sea and because the EAC is responsible for the largest oceanic inflow of volume.
The timeseries of Eulerian volume transport are not equal to the Lagrangian transport timeseries. The difference between the two methods is made visible in the 5-year means in Figure 14. The 5-year mean of the Lagrangian and Eulerian volume transport is also plotted as a reference. The Eulerian volume transport is larger than the Lagrangian volume transport. This is because the Lagrangian volume transport is only measured with the parcels that originate in the EAC seeding location, while the Eulerian transport is the total volume transport over the cross section. The Eulerian volume transport means are calculated with only the flow that is going in the direction of the current, so eastward for the TF and westward for the TL. The flow in opposite direction is the recirculation of the current, and is not accounted for in the Eulerian transport.
The difference between the Eulerian and the Lagrangian transports can be partly explained by the recirculation within the cross section. If a parcel in the Lagrangian simulation recirculates over the cross section, like in Figure 15, it is only counted the in the first time step of the crossing. When it recirculates back over the cross section, it is identified as local recirculating water and not as a connection between the EAC and the cross section. However, this is captured in the Eulerian volume transport. Eulerian method does not allow to selectively measure volume transport based on information of the location at the previous time steps of that parcel. It only 'sees' the total amount of volume transport that travels past its measuring point at that moment in time and cannot distinguish between volume transports based on the origin of the water that moves across it.
To get a better picture of the extra volume transport in the Eulerian volume transport due to recirculation, the difference between the net Eulerian volume transport and the Lagrangian volume transport is shown in Figure 16. The Eulerian volume transport is calculated without distinguishing the direction of the flow within the cross section and therefore subs-tracts the volume transport of the recirculation of the volume transport of the main flow. The difference between the two methods is smaller than in Figure 14. The Lagrangian volume transport is not smaller than the Eulerian transports at each 5-year mean. The difference between the volume transport is likely caused by ocean transport that originates from a different source in the Tasman Sea than the EAC core flow. The small negative difference in the TF can be explained by a larger volume transport that travels in opposite direction of the flow compared to the Lagrangian volume transport. The net Eulerian volume transport is still positive in this case. Other possible sources could be an inflow of the Tasman Sea east of the EAC core, which likely ends up in the TF flow or an inflow from the the ACC or STF which likely ends up in the TL. A backward simulation of parcels seeded in each of the cross sections will identify the other origin locations.

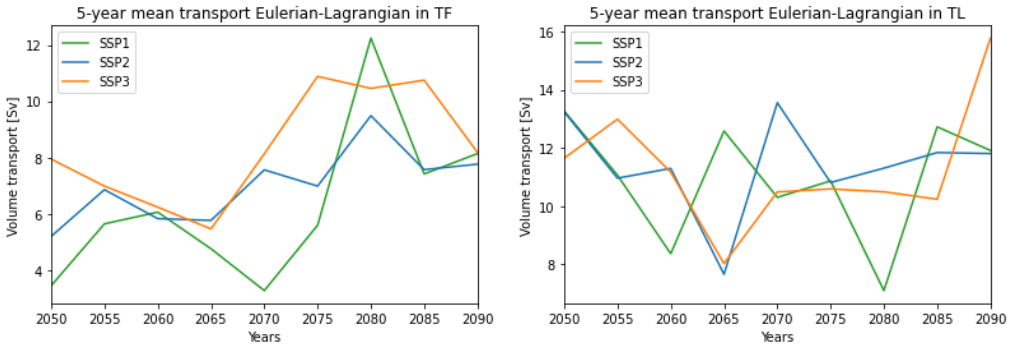

Figure 14: The 5-year mean of the Eulerian volume transport, calculated with only the direction of the flow, is plotted (–), together with the 5-year mean of the Lagrangian volume transport (-·-) for each of the climate scenarios. The difference between the two methods is plotted with a solid line. The difference between the Eulerian and Lagrangian volume transport can be explained by the recirculation of the current within the cross section.

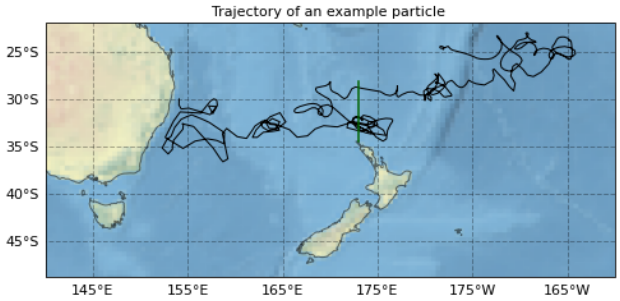

Figure 15: This figure shows a single trajectory of a parcel seeded in the EAC and crosses the TF cross section. In the Lagrangian time series of the volume transport, the volume transport of this parcel is only counted at the first time step it crosses the TF. In the Eulerian time series, the volume is captured in each time step. The eddy activity south of the separation point of the EAC is also visible in this figure.

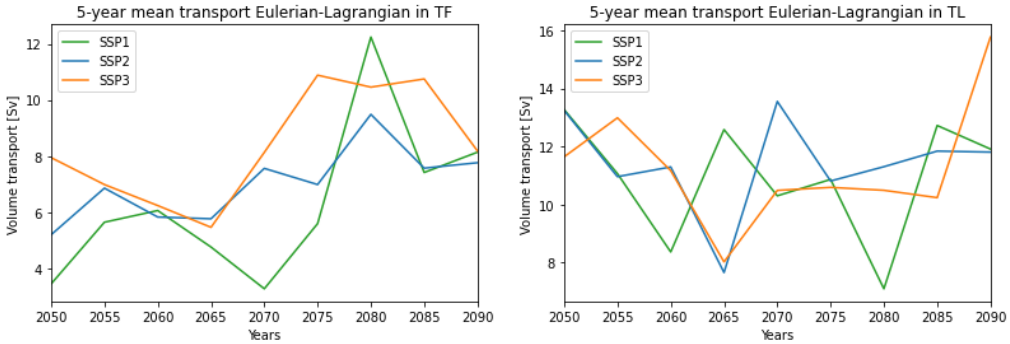

*Figure 16: The 5-year mean of the **net** Eulerian volume transport is plotted (–), together with the 5-year mean of the Lagrangian volume transport (-·-) for each of the climate scenarios. The difference between the two methods is plotted with a solid line. The recirculation within the cross section reduces the Eulerian volume transports shown in Figure 14. The difference between the Lagrangian possibly represents the volume transport that crosses the section but does not originate in the EAC.*

3.5 Connection with Westerly winds

The Lagrangian volume transport is correlated to the zonal mean of the wind stress over the South Pacific Ocean and the whole domain of the Southern Ocean. For the correlation the Pacific domain is defined between 130°E and 67°W, 10°S and 60°S.
The tables below show the correlation values between the zonal wind stress and the volume transport through the TF, TL and EAC. The p-values of the correlation are given between brackets. There is no obvious correlation between the Westerly winds and the Lagrangian transports and most correlation coefficients even have a high p-value. There is no time shift applied to the correlation and further research is needed to study the driver of the change. This will be further discussed in the conclusion and discussion section.

(a) TF

	Historical	SSP1	SSP2	SSP3
South Pacific				
Max value	0.043 (0.513)	-0.04 (0.322)	0.039 (0.339)	-0.021 (0.612)
Latitude	0.038 (0.567)	0.075 (0.066)	-0.05 (0.218)	0.056 (0.167)
Southern ocean				
Max value	0.047 (0.479)	-0.037 (0.359)	0.012 (0.761)	-0.061 (0.137)
Latitude	-0.073 (0.275)	0.071 (0.08)	-0.058 (0.159)	0.042 (0.307)

(b) TL

	Historical	SSP1	SSP2	SSP3
South Pacific				
Max value	0.073 (0.272)	0.085 (0.038)	0.076 (0.062)	0.14 (0.001)
Latitude	-0.033 (0.624)	0.031 (0.445)	-0.079 (0.053)	-0.06 (0.141)
Southern ocean				
Max value	-0.021 (0.758)	0.019 (0.65)	-0.036 (0.38)	0.031 (0.449)
Latitude	-0.147 (0.026)	-0.066 (0.105)	-0.182 (0.0)	-0.167 (0.0)

(c) EAC

	Historical	SSP1	SSP2	SSP3
South Pacific				
Max value	-0.016 (0.811)	0.13 (0.001)	0.15 (0.0)	0.191 (0.0)
Latitude	0.056 (0.396)	-0.048 (0.237)	0.012 (0.763)	-0.003 (0.945)
Southern ocean				
Max value	-0.04 (0.548)	0.014 (0.737)	0.055 (0.178)	0.051 (0.217)
Latitude	0.027 (0.688)	-0.096 (0.018)	-0.085 (0.037)	-0.133 (0.001)

Table 7: The correlation coefficients between the zonal wind stress and the TF, TL and EAC are shown in this table. All correlation values are below 0.2, with some very high p-values up to 0.95. No time-shift between the time series is applied.

4 Conclusion & discussion

We have shown that a Lagrangian analysis applied within NZESM gives us a better understanding of the Tasman Sea and the connectivity between regions. We are able to study the currents in more detail and visualise the volume and temperature transports
NZESM is a fully coupled earth system model [Behrens et al., 2020] based on UKESM [Kuhlbrodt et al., 2018], and is used to evaluate the volume and temperature transport in the Tasman Sea. NZESM contains a historical simulation from 1950-2014 and covers three future climate scenarios. A low-emission scenario, SSP1, a high-emission scenario SSP3 and a middle-road scenario SSP2. The volume transports of several cross sections in the Tasman Sea are compared to other studies and a hindcast model NZ20 to validate NZESM. We can conclude that NZESM gives good representation of the advection in western boundary current system in the Tasman Sea, with the exception of the SC. The SC flows around the New Zealand's South Island over the eastern shelf break with uneven bathymetry that influences the currents [P. Sutton, 2001]. The $1/5°$ resolution might still be to coarse to fully represent the bathymetry in the region correctly.
OceanParcels is used to compute a Lagrangian analysis and study the connectivity between the EAC and the rest of the Tasman Sea. Parcels were seeded in the EAC at 30°S in a historical simulation from 1950-2014 and 3 future climate pathways from 2030-2100, using a continuous seeding strategy with a 5 day interval. After a simulation of 70 years, between 98% and 99.8% of the parcels have exited the Tasman Sea for all simulations. The parcels that have not crossed one of the exit cross sections, could still be moving through the Tasman Sea, be stuck along the coastline, or have reached the ocean surface and evaporated. The different simulations, confirm that enough parcels have been seeded and results are not influenced by a lack of seeded parcels. Therefore the fact that only 1.5% - 2% of the parcels get stuck in the Tasman Sea is assumed not to affect the outcome of the results significantly.

A timeseries of the volume transport through the cross section in the Tasman Sea is computed using an Eulerian and Lagrangian analysis. Both the Eulerian and Lagrangian analysis show a shift in volume transport from the TF to the TL in both SSP2 and SSP3. With the largest changes in SSP3. A time series of the transports show that the decrease of volume transport through the TF and TL highly depend on the emission scenario.
The mean volume transports calculated with the Eulerian analysis, show an increase of volume transport through the TL and the TF in SSP1, a small decrease through the TF and increase through the TL in SSP2 and a large shift in volume transport from the TF to the TL in SSP3. The mean of the volume and temperature transport for both the Eulerian and Lagrangian analysis are calculated over multiple decades to account for interdecadal variability of the currents. The change in volume transport does not affect the width of the TL and TF. The increase of the TL is caused by an intensification of the velocities, which is in contrast with the increase in transport in the Agulhas current, which is weakening and broadening [Beal and Elipot, 2016]. Beal et al., [2016] found that this broadening of the Agulhas current can be explained by an increase inn eddy kinetic energy (EKE) and meanders within the current that transfer energy further off shore. The separation of the EAC in the TF and EAC extension is also based on EKE, so a next interesting step would be to study the broadening of the EAC-extension and the connection of the shift in volume transport and EKE. A small increase in the variability of the TL in the high emission scenario

is visible in Figure 8. Which could suggest an increase in eddy activity. The southern point of the TL cross section is located near the STF. This might be a factor what the TL does not broaden despite an increase in the current strength, as it might work as a boundary that contains the width of the current. Further study is needed to identify the mechanism of the intensification of TL and the contrast between the EAC and the Agulhas current.

The volume transports, computed with the Lagrangian analysis, in the historical simulation show a downward trend for the TF and an upward trend for the TL. This agrees with the studies conducted about the spin up of the South Pacific super gyre in the past few decades [Oliver et al., 2014], [Cai et al., 2005]. However, there is a large sudden decrease in the volume transport in the TF around 2000, which increases again around 2010. This interdecadal variation could cause this downward trend as the trend of the volume transport in the SSP1 scenario has a higher average compared to the historical period. This could also suggest an increase in volume transport in the first half of the 21^{st} century through the TF. To account for this variability, the Lagrangian simulation can be performed for different ensembles of NZESM. And a simulation that spans over the whole time frame from 1950 until 2100.
The mean Lagrangian volume and temperature transports are calculated between 2050-2100 to account for the interdecadal variability and as 5-yearly means to study the trend. The volume transport through the TF and TL in SSP1, over the second half of this century show a small increase. The TF increases between 2050-2075 and then decreases between 2075-2100, while the TL shows a increasing trend between 2050-2100. In SSP2, the volume transport through the TF decreases 10% and increases 54% for the TL. In SSP3, the largest shift in volume transport from the TF towards the TL is also visible in the Lagrangian analysis. The volume transport through the TF decreases 33% and increases by 76% for the TL. The Lagrangian volume and temperature transport is coupled, and shows the same tendency in each of the cross sections. Towards the TL, the temperature transport increases in all future scenarios compared to the historical simulation, with a more extreme increase in the high emission scenario compared to the historical period. In the high emission scenario, there is a decrease in temperature transport towards New Zealand. However, the temperature transport decreases with a smaller rate than the volume transport. The decrease in temperature transport in through the TF in the high emission scenario, was not expected. As in this scenario, marine heat waves intensify significantly north of New Zealand [Behrens et al., 2022]. The Lagrangian trajectory pathways displayed in Figure 12 show a decrease in volume and temperature transport in this region north of New Zealand in SSP3. A possible explanation for the contradiction between intensifying marine heat waves as described in Behrens et al., [2022] and a decrease in temperature transport is that heat might be able to accumulate in the area north of New Zealand, due to the decrease in volume transport. The depth to which the marine heat waves penetrate are normally a first indication of the driver. If the temperature anomalies stretch to deeper depth below the mixed layer, it suggest they can be driven by ocean currents transporting the heat to the region [Elzahaby et al., 2021]. However, the Tasman Front is a surface intensified current and becomes more shallow in the high emission scenario. So the depth of the temperature anomalies in the region, does not straight away clarify the driver. A Lagrangian study that investigates the ocean temperature transport in and out of the region combined with the net atmospheric heat uptake, could help to investigate if the ocean transport or the atmospheric forcing is the dominant driver

of these projected marine heat waves.

The temperature along the trajectories between the EAC and the TF are increasing. By the end of this century, there is an increase in the fraction of volume weighted trajectories above 15°C and 20°C in the high emission scenario compared to the low emission scenario. At the end of the 20^{th} century, in the historical simulation, only 1% of the volume weighted trajectories towards New Zealand are above 20°C, this increases to 5.5% by the end of the 21^{st} century for the high emission scenario. Despite a decline in the overall Lagrangian temperature transport, the volume weighted fraction of trajectories which encounter higher temperatures from the EAC to the north of NZ increases. This method can be applied to study the potential of opening or widening pathways for invasive species to arrive in New Zealand by passive transport. The Lagrangian volume transport trajectories are material pathways and volume is conserved. However, the mixing of tracers between trajectories is possible and is dependent on the biological species. The depth of the trajectory can be tracked as well, which allows the study of the survival of biota that is influenced by the amount of available light. This is not covered in the scope of this study, but is a possible application of this research.

No significant correlation between change in strength of the westerly winds and the volume transport through the cross sections was found in this study. This could be caused by a time delay between the wind stress and the current strength. The correlation could improve when a time shift is applied to the time series of either the wind stress or the volume transport of the cross section. Winds affect the ocean circulation, but at the same time are the large scale winds influenced by the ocean. Simply shifting the timeseries until a high correlation is found, does not straight away prove the causal relation of the driver. Bull et al., [2017] found that the variability of western boundary currents is driven by local wind changes which generates baroclinic instabilities. These instabilities create eddies who in their turn affect the variability of the current. A correlation between the local wind stress over the Tasman Sea and the time series of the current can be performed to find the location that affects the variability in the current. Further study needs to be done to find out if the strength or the poleward shift of the Westerly winds has an effect on the spin-up of the South Pacific gyre.

References

Beal, L. M., Elipot, S. (2016, November 9). Broadening not strengthening of the Agulhas Current since the early 1990s. *Nature, 540(7634), 570–573.* https://doi.org/10.1038/nature19853

Behrens, E., Fernandez, D., Sutton, P. (2019, May 7). Meridional Oceanic Heat Transport Influences Marine Heatwaves in the Tasman Sea on Interannual to Decadal Timescales. *Frontiers in Marine Science, 6.* https://doi.org/10.3389/fmars.2019.00228

Behrens, E., Williams, J., Morgenstern, O., Sutton, P., Rickard, G., Williams, M. J. M. (2020). Local Grid Refinement in New Zealand's Earth System Model: Tasman Sea Ocean Circulation Improvements and Super-Gyre Circulation Implications. *Journal of Advances in Modeling Earth Systems, 12(7).* https://doi.org/10.1029/2019ms001996

Behrens, E., Hogg, A. M., England, M. H., Bostock, H. (2021). Seasonal and Interannual Variability of the Subtropical Front in the New Zealand Region. *Journal of Geophysical Research: Oceans, 126(2).* https://doi.org/10.1029/2020jc016412

Behrens, E., Rickard, G., Rosier, S., Williams, J., Morgenstern, O., Stone, D. (2022). Projections of Future Marine Heatwaves for the Oceans Around New Zealand Using New Zealand's Earth System Model. Frontiers in Climate, 4. https://doi.org/10.3389/fclim.2022.798287

Bull, C. Y. S., Kiss, A. E., Jourdain, N. C., England, M. H., van Sebille, E. (2017, December). Wind Forced Variability in Eddy Formation, Eddy Shedding, and the Separation of the East Australian Current. Journal of Geophysical Research: Oceans, 122(12), 9980–9998. https://doi.org/10.1002/2017jc013311

Cai, W., Shi, G., Cowan, T., Bi, D., Ribbe, J. (2005). The response of the Southern Annular Mode, the East Australian Current, and the southern mid-latitude ocean circulation to global warming. Geophysical Research Letters, 32(23). https://doi.org/10.1029/2005gl024701

Chiswell, S. M., Rickard, G. J. (2006, October 20). Comparison of model and observational ocean circulation climatologies for the New Zealand region. *Journal of Geophysical Research, 111(C10).* https://doi.org/10.1029/2006jc003489

Chiswell, S. M., Bostock, H. C., Sutton, P. J., Williams, M. J. (2015, April 3). Physical oceanography of the deep seas around New Zealand: a review. *New Zealand Journal of Marine and Freshwater Research, 49(2), 286–317.* https://doi.org/10.1080/00288330.2014.992918

Ekman, V., 1905: On the influence of the Earth's rotation on ocean-currents. *Ark. Mat. Astron. Fys., 2, 1–53.*

Elzahaby, Y., Schaeffer, A., Roughan, M., Delaux, S. (2021). Oceanic Circulation Drives the Deepest and Longest Marine Heatwaves in the East Australian Current System. *Geophysical Research Letters, 48(17).* https://doi.org/10.1029/2021gl094785

Fernandez, D., Bowen, M., Sutton, P. (2018). Variability, coherence and forcing mechanisms in the New Zealand ocean boundary currents. *Progress in Oceanography, 165,* 168–188. https://doi.org/10.1016/j.pocean.2018.06.002

Godfrey, J. S., G. R. Cresswell, T. J. Golding, and A. F. Pearce (1980), The separation of the East Australian Current, *J. Phys. Oceanogr., 10, 430–439*

Good, S. A., Martin, M. J., Rayner, N. A. (2013). EN4: Quality controlled ocean temperature and salinity profiles and monthly objective analyses with uncertainty estimates. *Journal of Geophysical Research: Oceans, 118, 6704–6716.* https://doi.org/10.1002/2013JC009067

Hunke, E., Lipscomb, W., Jones, P., Turner, A., Jeffery, N., and Elliott, S. (2017). CICE: *The Los Alamos Sea Ice Model (No.CICE: 005315WKSTN00).* Los Alamos, NM: Los Alamos National Lab

Kuhlbrodt, T., Jones, C. G., Sellar, A., Storkey, D., Blockley, E., Stringer, M., Hill, R., Graham, T., Ridley, J., Blaker, A., Calvert, D., Copsey, D., Ellis, R., Hewitt, H., Hyder, P., Ineson, S., Mulcahy, J., Siahaan, A., Walton, J. (2018, November). The Low-Resolution Version of HadGEM3 GC3.1: Development and Evaluation for Global Climate. *Journal of Advances in Modeling Earth Systems, 10(11), 2865–2888.* https://doi.org/10.1029/2018ms001370

Loveday, B. R., Penven, P., Reason, C. J. C. (2015). Southern Annular Mode and westerly-wind-driven changes in Indian-Atlantic exchange mechanisms. *Geophysical Research Letters, 42(12), 4912–4921.* https://doi.org/10.1002/2015gl064256

Madec, G., Bourdallé-Badie, R., Bouttier, P. A., Bricaud, C., Bruciaferri, D., Calvert, D., et al. (2017). *NEMO Ocean Engine.*

Marsh,R, & van Sebille, E.V. (2021) *Ocean Currents: physical Drivers in a Changing World*(1^{st} ed). Elsevier

Matear, R. J., Chamberlain, M. A., Sun, C., Feng, M. (2013). Climate change projection of the Tasman Sea from an Eddy-resolving Ocean Model. Journal of *Geophysical Research: Oceans, 118(6), 2961–2976.* https://doi.org/10.1002/jgrc.20202

MUNK, W. H., CARRIER, G. F. (1950, August). The Wind-driven Circulation in Ocean Basins of Various Shapes. *Tellus, 2(3), 160–167.* https://doi.org/10.1111/j.2153-3490.1950.tb00327.x

Lorrey, A. M., Bostock, H. (2016, December 17). The Climate of New Zealand Through the Quaternary. *Landscape and Quaternary Environmental Change in New Zealand, 67–139.* https://doi.org/10.2991/978-94-6239-237-3_3

O'Neill, B. C., Kriegler, E., Riahi, K., Ebi, K. L., Hallegatte, S., Carter, T. R., Mathur, R., van Vuuren, D. P. (2013). A new scenario framework for climate change research: the concept of shared socioeconomic pathways. *Climatic Change, 122(3)*, 387–400. https://doi.org/10.1007/s10584-013-0905-2

Oke, P. R., Roughan, M., Cetina-Heredia, P., Pilo, G. S., Ridgway, K. R., Rykova, T., Archer, M. R., Coleman, R. C., Kerry, C. G., Rocha, C., Schaeffer, A., Vitarelli, E. (2019, September). Revisiting the circulation of the East Australian Current: Its path, separation, and eddy field. *Progress in Oceanography, 176, 102139.* https://doi.org/10.1016/j.pocean.2019.102139

Oliver, E. C. J., Holbrook, N. J. (2014). Extending our understanding of South Pacific gyre "spin-up": Modeling the East Australian Current in a future climate. *Journal of Geophysical Research: Oceans, 119(5), 2788–2805.* https://doi.org/10.1002/2013jc009591

Qu, T., Fukumori, I., Fine, R. A. (2019, January). Spin-Up of the Southern Hemisphere Super Gyre. Journal of Geophysical Research: Oceans, 124(1), 154–170. https://doi.org/10.1029/2018jc014391

Rae, J. G. L., Hewitt, H. T., Keen, A. B., Ridley, J. K., West, A. E., Harris, C. M., et al. (2015). Development of the Global Sea Ice 6.0 CICE configuration for the Met Office Global Coupled model. Geosci. Model Dev. 8, 2221–2230. doi: 10.5194/gmd-8-2221-2015

Ridgway, K., Dunn, J. (2003). Mesoscale structure of the mean East Australian Current System and its relationship with topography. *Progress in Oceanography, 56(2),* 189–222. https://doi.org/10.1016/s0079-6611(03)00004-1

Ridgway, K. R. (2007, July 14). Long-term trend and decadal variability of the southward penetration of the East Australian Current. Geophysical Research Letters, 34(13), n/a-n/a. https://doi.org/10.1029/2007gl030393

Roemmich, D., Sutton, P. (1998, June 15). The mean and variability of ocean circulation past northern New Zealand: Determining the representativeness of hydrographic climatologies. Journal of Geophysical Research: Oceans, 103(C6), 13041–13054. https://doi.org/10.1029/98jc00583

Salinger, M. J., Renwick, J., Behrens, E., Mullan, A. B., Diamond, H. J., Sirguey, P., Smith, R. O., Trought, M. C. T., Alexander, L., Cullen, N. J., Fitzharris, B. B., Hepburn, C. D., Parker, A. K., Sutton, P. J. (2019, April 12). The unprecedented coupled ocean-atmosphere summer heatwave in the New Zealand region 2017/18: drivers, mechanisms and impacts. Environmental Research Letters, 14(4), 044023. https://doi.org/10.1088/1748-9326/ab012a

Sen Gupta, A., Stellema, A., Pontes, G. M., Taschetto, A. S., Vergés, A., Rossi, V. (2021). Future changes to the upper ocean Western Boundary Currents across two generations of climate models. *Scientific Reports, 11(1).* https://doi.org/10.1038/s41598-021-88934-w

Shimura, T., Pringle, W. J., Mori, N., Miyashita, T. Yoshida, K. (2022, 18 maart). Seamless Projections of Global Storm Surge and Ocean Waves Under a Warming Climate. *Geophysical Research Letters, 49(6).* https://doi.org/10.1029/2021gl097427

Sutton, P. (2001, December 15). Detailed structure of the Subtropical Front over Chatham Rise, east of New Zealand. Journal of Geophysical Research: Oceans, 106(C12), 31045–31056. https://doi.org/10.1029/2000jc000562

Sutton, P. J. H. (2003). The Southland Current: A subantarctic current. *New Zealand Journal of Marine and Freshwater Research, 37(3),* 645–652. https://doi.org/10.1080/00288330.2003.9517195

Trenberth, K. E. (2007, July). Warmer Oceans, Stronger Hurricanes. Scientific American, 297(1), 44–51. https://doi.org/10.1038/scientificamerican0707-44

van Sebille, E., England, M. H., Zika, J. D., Sloyan, B. M. (2012, March 24). Tasman leakage in a fine-resolution ocean model. *Geophysical Research Letters, 39(6).* https://doi.org/10.1029/2012gl051004

van Sebille, E., Griffies, S. M., Abernathey, R., Adams, T. P., Berloff, P., Biastoch, A., Blanke, B., Chassignet, E. P., Cheng, Y., Cotter, C. J., Deleersnijder, E., Döös, K., Drake, H. F., Drijfhout, S., Gary, S. F., Heemink, A. W., Kjellsson, J., Koszalka, I. M., Lange, M., . . . Zika, J. D. (2018). Lagrangian ocean analysis: Fundamentals and practices. *Ocean Modelling, 121, 49–75.* https://doi.org/10.1016/j.ocemod.2017.11.008

Walters, D., Baran, A. J., Boutle, I., Brooks, M., Earnshaw, P., Edwards, J. (2019). The met office unified model global atmosphere 7.0/7.1 and JULES Global Land 7.0 configurations. *Geosci. Model Dev. 12, 1909–1963.* doi: 10.5194/gmd-2017-291-AC2

Yool, A., Popova, E. E., Anderson, T. R. (2013, October 29). MEDUSA-2.0: an intermediate complexity biogeochemical model of the marine carbon cycle for climate change and ocean acidification studies. *Geoscientific Model Development, 6(5), 1767–1811.* https://doi.org/10.5194/gmd-6-1767-2013

Ypma, S. L., van Sebille, E., Kiss, A. E., Spence, P. (2016, January). The separation of the East Australian Current: A Lagrangian approach to potential vorticity and upstream control. *Journal of Geophysical Research: Oceans, 121(1), 758–774.* https://doi.org/10.1002/2015jc011133

A Appendix

A.1 Animation

The advection of the particles of the simulation with U & V and with U,V and W are made visible in an animation. These can be downloaded from the following link:

https://tinyurl.com/bddhmd7z

In the simulation with only U & V, more particles get stuck along the coast of Australia, Tasmania and New Zealand's North island. There are still a few particles in the simulation with U, V & W velocities that get stuck. In Section 3.2, we see that around 1.7-2% of parcels are still in the Tasman Sea. The particles that are seen stuck in the animation, could explain part of this 2%. Studying the distance travelled of each particle in each time step can explain the amount of particles that are stuck. But as this is only a small amount, this is not performed in this study.

A.2 Eulerian cross sections

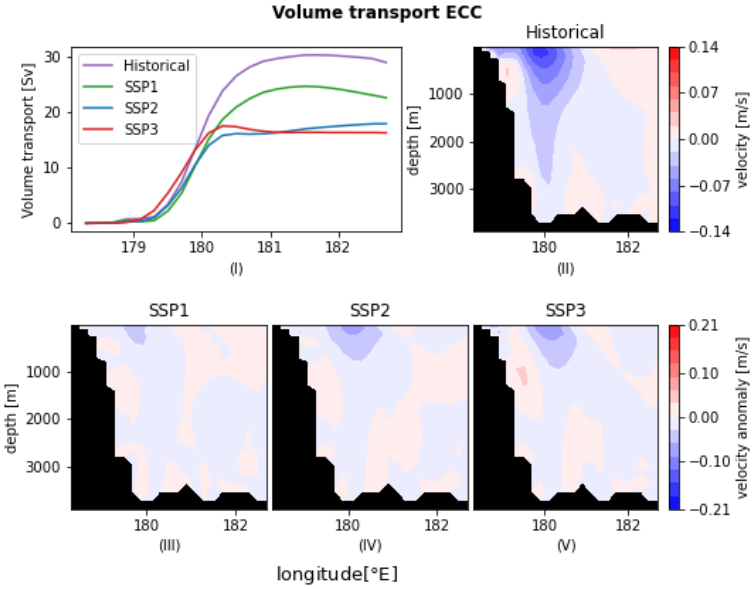

(a)

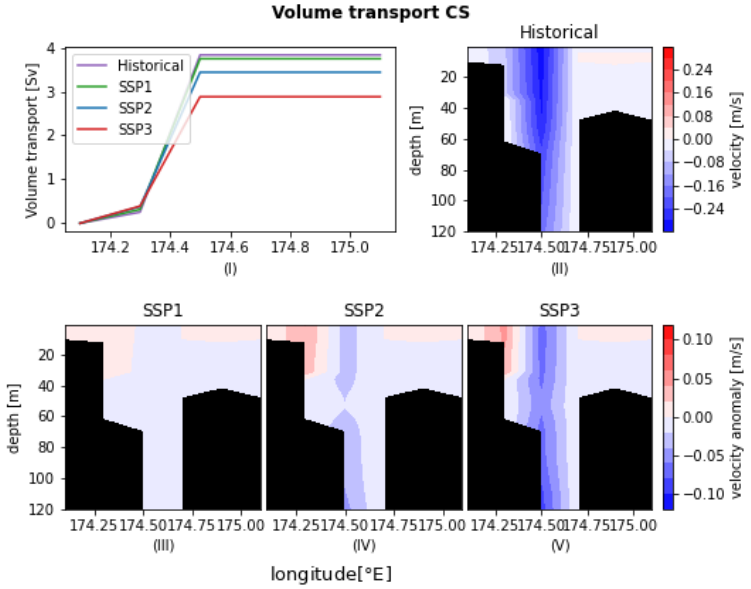

(b)

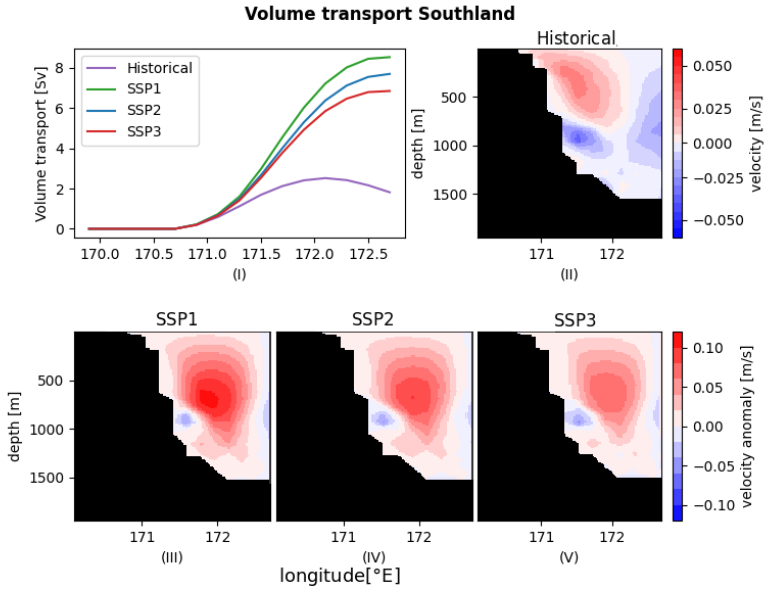

(c)

Figure 17: The Eulerian cross sections per future emission scenario. Sub-figure (I) in each of the figures is the sum of the current calculated from the coast outward to the ocean end of the cross section. The mean velocities of the historical simulation are plotted in Sub-figure (II). The contour plots in Sub-figure (III), (IV) and (V), show the anomalies of each of the future emission scenarios compared to the reference period. Positive anomalies mean an increase in velocities and negative anomalies a decrease and they indicate the location of the largest change.

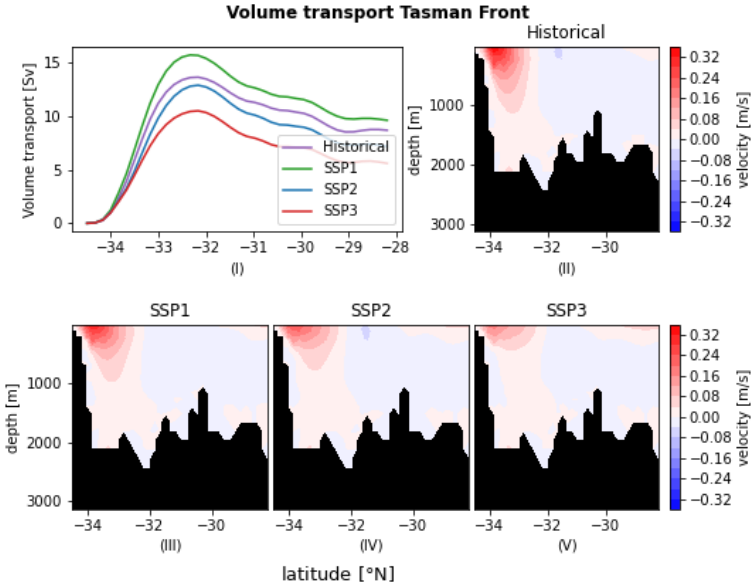
Volume transport Tasman Front
Historical
SSP1
SSP2
SSP3
Volume transport [Sv]
depth [m]
velocity [m/s]
(I)
(II)
(III)
(IV)
(V)
latitude [°N]

(a)

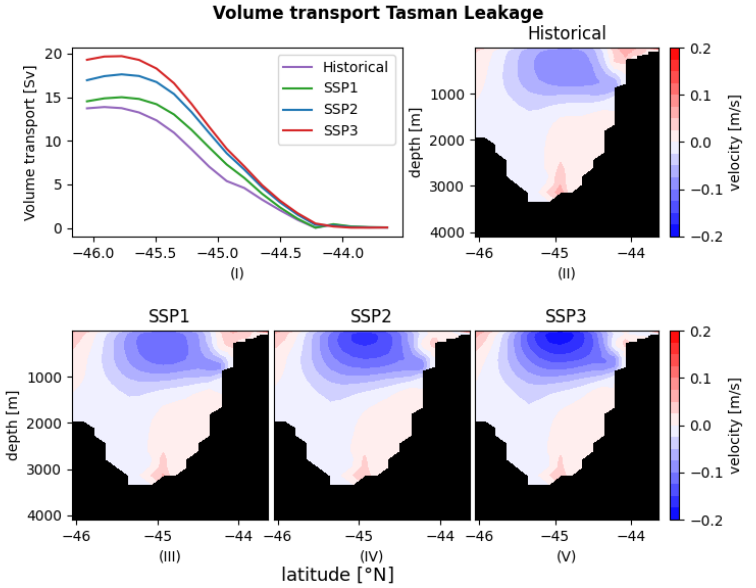
Volume transport Tasman Leakage
Historical
SSP1
SSP2
SSP3
Volume transport [Sv]
depth [m]
velocity [m/s]
(I)
(II)
(III)
(IV)
(V)
latitude [°N]

(b)

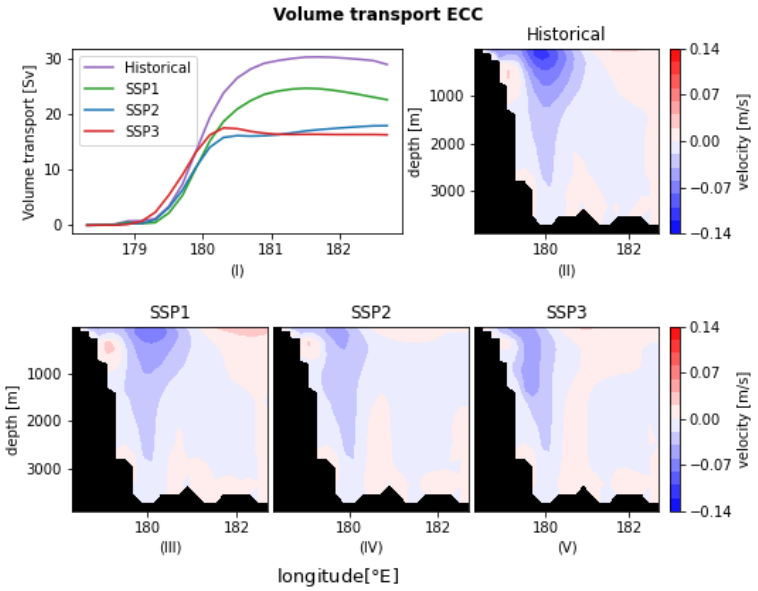

(c)

Figure 18: Sub-figure (I) and (II) are identical to Figure 5 for the TL, TF and ECC. Sub-figure (III), (IV) and (V) show the mean velocities of the future scenarios instead of the anomalies. It shows the change in shape of the current. For the TF, the current becomes more surface intensified. The TL intensifies by increasing velocities, but the width or shape of the current does not change significantly. The ECC slows down and becomes more narrow as was also visible in sub-figure (I).

A.3 Closed Box

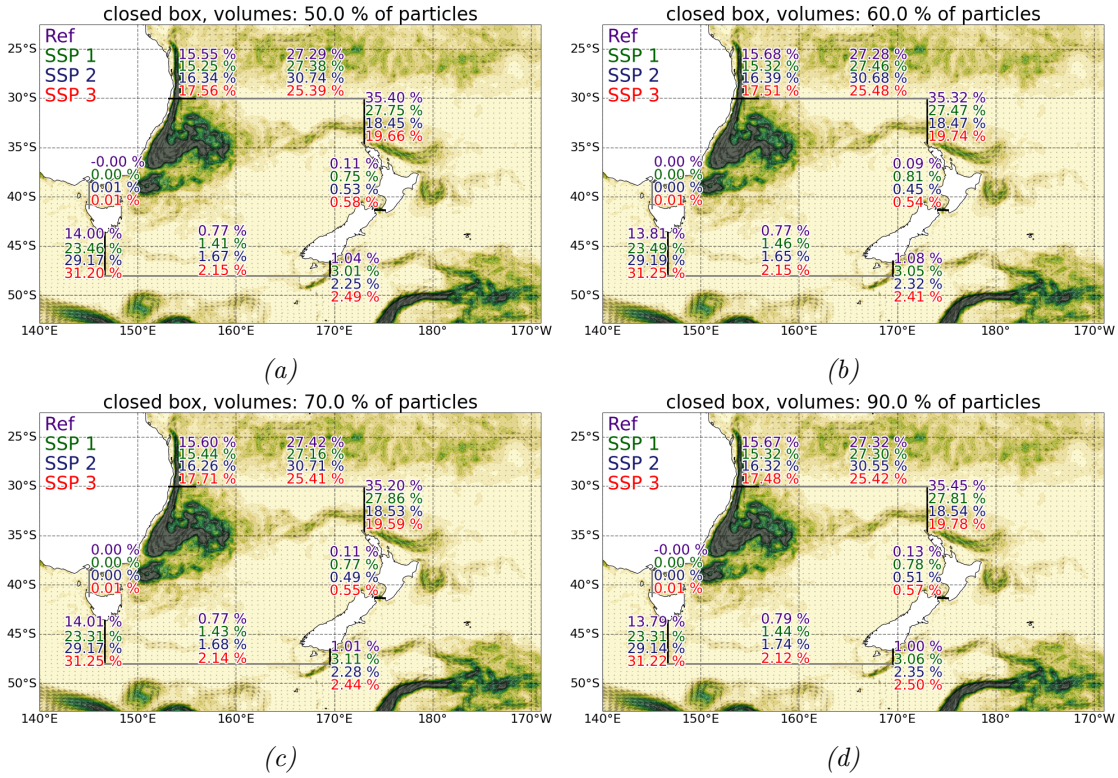

Figure 19: The results of random selected parcels for 50%,60%,70%,90% of the parcels. The distribution of the exiting particles out of the Tasman Sea does not change, which means that we seed enough parcels within the EAC cross section.

A.4 Time series

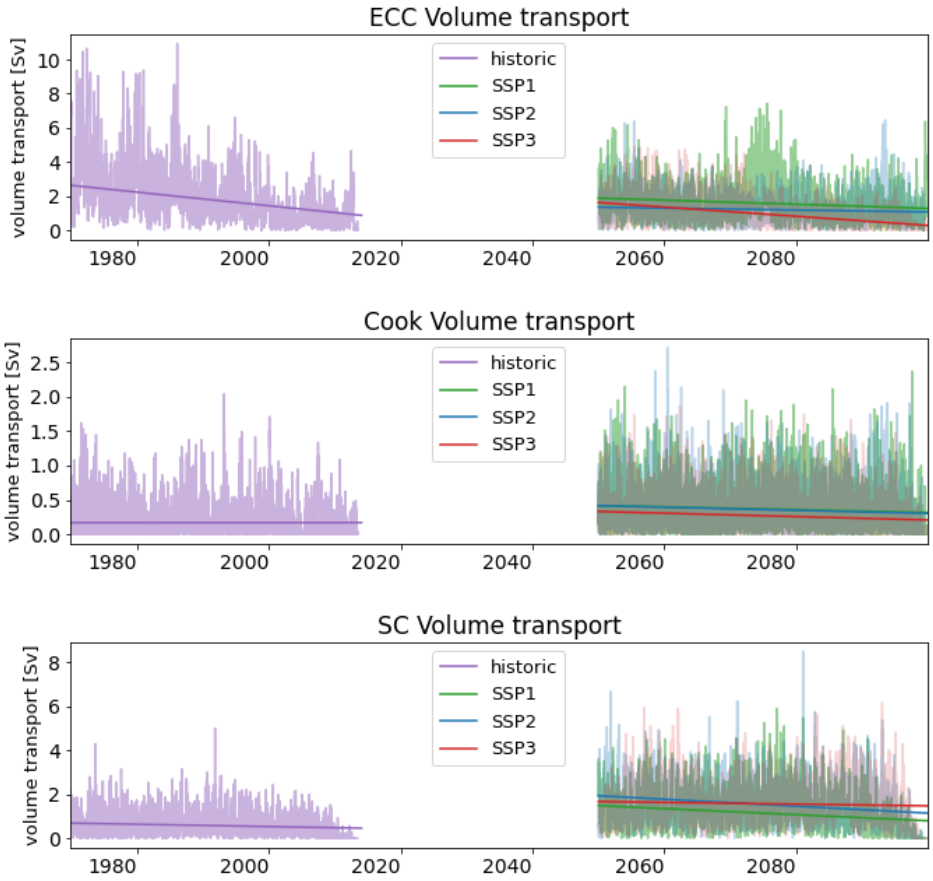

Figure 20: The volume transport through the cross section for the ECC, CS and SC are plotted for the historical simulation from 1970-2014 and the future scenarios from 2050-2100. The line fit shows the trend of the current. The volume transport through the ECC decreases the most in the the high emission scenario, which follows the Eulerian trend and the trend through the TF. The CS does not show a large increase or decrease. Interesting to note is that the mean Lagrangian transports are a factor 5-10 times smaller than the Eulerian transports. The volume transports through the SC show a small increase over the three climate scenarios, but stay fairly constant over the time series. The increase is likely a cause of the incorrect representation of the currents within the region, as seen in the Eulerian means. We can therefore not make any conclusions on how the current alters in the future based on these Lagrangian timeseries.

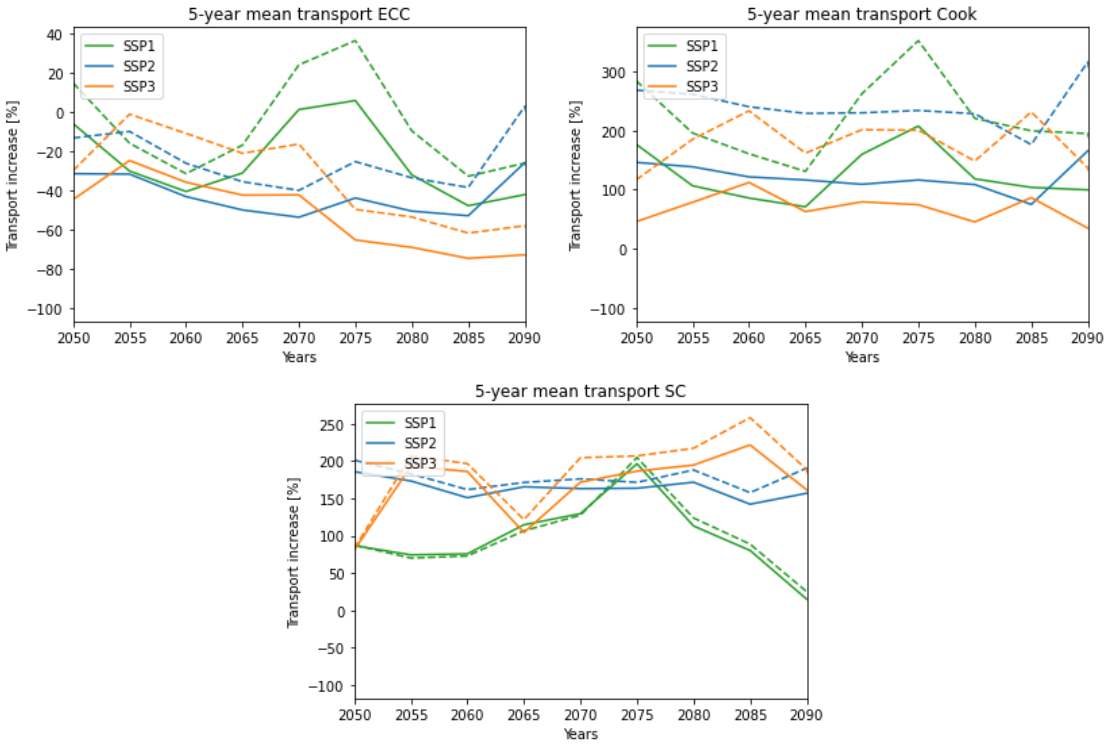

Figure 21: The 5-year mean of the volume and temperature transport anomaly through the ECC, CS and SC are given compared to the historical mean in percentages. The volume transport and temperature transport are coupled, which corresponds with the 5-year means of the EAC, TF and TL. The CS shows a large increase, but as the current has low volume transports, this might give a distorted image of what is actually happening.